Cleaner Energy Systems 13 (2026) 100246

Contents lists available at ScienceDirect

Cleaner Energy Systems

journal homepage: www.elsevier.com/locate/cles

Hybrid micro-compressed air energy storage with photovoltaic and diesel generation for off-grid applications: A parametric life cycle and techno-economic study

Dario Tumminello *, Claudio Zuffi, Tommaso Bacci, Bruno Facchini

Department of Industrial Engineering DIEF, University of Florence, Via di Santa Marta 3, Florence, 50139, Italy

ARTICLE INFO

Keywords:
Compressed air energy storage
Life cycle assessment
Techno-economic optimization

ABSTRACT

Reliable and sustainable electricity supply remains a major challenge for remote off-grid communities, which often rely on costly and carbon-intensive diesel generators. Decarbonizing these areas requires the integration of renewable energy technologies with storage solutions to mitigate the variability and intermittency of renewable power production. This study aims to investigate the potential of micro-scale Compressed Air Energy Storage (micro-CAES) to improve the environmental and economic performance of hybrid photovoltaic (PV)–diesel systems under realistic operating conditions. A dynamic, system-level thermodynamic model is coupled with an optimization framework to determine the optimal sizing of photovoltaic and storage components according to alternative objective functions. A key aspect of this work lies in the integration of this optimization with a parametric cradle-to-grave Life Cycle Assessment, enabling the consistent evaluation of environmental impacts as a function of system size. Environmental performance is assessed using Global Warming Potential (GWP), while economic viability is evaluated through the Levelized Cost of Energy (LCOE). Three system configurations, namely diesel-only, PV–diesel, and PV–diesel–CAES, are analyzed for seven representative off-grid locations with differing solar resource availability and diesel price levels. Results show that replacing diesel generation with photovoltaic systems reduces greenhouse gas emissions from 0.996 to approximately 0.598 $kgCO_2eq/kWh$. The integration of micro-CAES enables further reductions, reaching 0.144–0.247 $kgCO_2eq/kWh$ depending on site conditions. From an economic perspective, the results indicate that the viability of PV–diesel–CAES systems is primarily driven by system size, diesel fuel price, and site-specific photovoltaic potential. In general, limited round-trip efficiency leads to photovoltaic oversizing and increased capital costs, which tend to outweigh fuel savings. As a result, storage integration becomes advantageous only in scenarios characterized by high diesel prices, where reduced generator operation compensates for the relatively low round-trip efficiency and the capital cost of the storage system. Overall, this work provides a comprehensive techno-economic and environmental assessment of micro-CAES-based hybrid systems for off-grid applications, highlighting their potential for substantial emission reductions while clearly identifying the conditions under which economic competitiveness can be achieved.

1. Introduction

1.1. Context

The increasing deployment of renewable energy sources highlights the need for storage technologies that ensure a stable and reliable electricity supply (Mohler and Sowder, 2017). Storage expansion is essential for decarbonization, and the European Commission identifies storage as a key enabler for the 2050 climate targets (Zakeri and Syri, 2015). The current reliance on lithium-ion batteries raises concerns about long-term scalability, sustainability, and resilience due to critical raw material constraints, environmental impacts, and geopolitical risks in lithium, cobalt, and nickel supply chains (Weil and Ziemann, 2014; Bleicher and Pehlken, 2020; Xu et al., 2022). Resource-based assessments indicate that, even with optimistic assumptions on technological progress and recycling, battery-centric storage alone may be insufficient for deep decarbonization, underscoring the need for a diversified portfolio of storage technologies with different material requirements (Bleicher and Pehlken, 2020; Söltzer et al., 2026; Deng et al., 2024). Among electrical energy storage options, Compressed Air

* Corresponding author.
E-mail address: dario.tumminello@unifi.it (D. Tumminello).

https://doi.org/10.1016/j.cles.2026.100246
Received 25 November 2025; Received in revised form 12 February 2026; Accepted 17 March 2026
Available online 18 March 2026

Nomenclature

Latin Symbols

A	Area (m^2)
C	Cost (economic) ($)
C	Heat capacity rate (thermodynamics) (W/K)
c_p	Constant pressure heat capacity (J/(kg K))
C_r	Thermal capacity ratio (–)
D	Diameter (m)
d	Discount rate (–)
E	Energy (J)
h	Specific enthalpy (J/kg)
I	Irradiance (W/m^2)
I_{STC}	Irradiance at standard test conditions (1000 W/m^2)
k	Thermal conductivity (W/(m K))
l	Length (m)
P	Power (W)
p	Pressure (Pa)
$P_{PV,p}$	Photovoltaic peak power (kWp)
R	Gas constant (J/(kg K))
T	Temperature (°C)
U	Internal energy (J)
U	Overall heat transfer coefficient (heat exchanger) (W/m^2K)
u	Specific internal energy (J/kg)
UA	Global heat transfer conductance (W/K)
V	Volume (m^3)
v	Specific volume (m^3/kg)
V_s	Swept volume (m^3)
Y	System lifetime (year)
m	Mass (kg)
$\dot{m}$	Mass flow rate (kg/s)
$\dot{Q}$	Heat flow rate (W)

Greek Symbols

α	Convective heat transfer coefficient (W/m^2K)
β	Pressure ratio (–)
δ	Wall thickness (m)
η	Efficiency (–)
γ	Heat capacity ratio (–)
ρ	Density (kg/m^3)
σ	Standard deviation (statistics) (unit of the variable)
σ	Stress (mechanical engineering) (MPa)
σ_y	Yield stress (MPa)
σ_{all}	Allowable stress (MPa)
ε	Heat exchanger efficiency (–)

Subscripts and Superscripts

ad	Adiabatic
amb	Ambient conditions or to/from the ambient
c	Compressor
DG	Diesel generator
ex	Expander
in	Inlet
is	Isentropic
L	End user load
max	Maximum value
min	Minimum value
n	Nominal condition
out	Outlet
ref	Reference value
vol	Volumetric

Acronyms

AC	Annual cost ($)
AR	Aspect ratio (–)
CAES	Compressed Air Energy Storage
CAPEX	Capital Expenditure
CAS	Compressed Air Storage
CEPCI	Chemical Engineering Plant Cost Index
EGO	Efficient Global Optimization
ER	Energy Resources depletion (MJ/kWh)
FE	Freshwater Eutrophication (kg P eq/kWh)
FET	Freshwater Eco-Toxicity (CTUe/kWh)
GWP	Global Warming Potential (kg CO_2 eq/kWh)
HEX	Heat Exchanger
HTC	Human Toxicity Carcinogenic (CTUh/kWh)
HTNC	Human Toxicity Non-Carcinogenic (CTUh/kWh)
IR	Ionizing Radiation (kBq U-235 eq/kWh)
LCA	Life Cycle Assessment
LCI	Life Cycle Inventory
LCIp	Parametric Life Cycle Inventory
LCOE	Levelized Cost of Energy ($/kWh)
LHV	Lower Heating Value (J/kg)
LU	Land Use (–)
ME	Marine Eutrophication (kg N eq/kWh)
MR	Mineral Resource Depletion (kg Sb eq/kWh)
NTU	Number of Transfer Units
OD	Ozone Depletion (kg CFC-11 eq/kWh)
PM	Particulate Matter Formation (disease incidence/kWh)
POF	Photochemical Oxidant Formation (kg NMVOC eq/kWh)
PR	Performance Ratio (–)
PV	Photovoltaic
RMSE	Root mean square error
RSS	Renewable Self Sufficiency (–)
RTE	Round Trip Efficiency (–)
SF	Safety Factor (–)
SS	Single Score
TE	Terrestrial Eutrophication (mol N eq/kWh)
TES	Thermal Energy Storage
WU	Water Use (m^3)

Note: some symbols are used with different meanings depending on the context.

Energy Storage (CAES) is attractive for long-duration storage. While originally developed for large-scale plants (King et al., 2021), CAES also shows potential at smaller scales (Petrov et al., 2013; Dehghani-Sanij et al., 2019), particularly in hybrid systems for remote areas combining renewables, storage, and diesel generators (Ibrahim and Ilinca, 2012). Diesel generation remains common in isolated communities; for instance, in Canada, about 200,000 people rely on diesel electricity, producing roughly 1.2 million tons of annual GHG emissions (Weis and Ilinca, 2008). Replacing diesel with renewables supported by storage is therefore essential. At the same time, it is essential to assess the environmental implications of different possible system configurations. In this context, the Life Cycle Assessment (LCA) methodology represents a relevant tool for such evaluations (Elzein et al., 2019).

1.2. State of the art

Given the extensive literature on CAES, this section is focused on studies assessing CAES feasibility for supplying stand-alone communities and those addressing life cycle assessment of such systems.

Early investigations on CAES for remote rural communities were conducted by Canadian research consortia between 2008 and 2015. After defining technical requirements for viable storage (Weis and Ilinca, 2008), these studies demonstrated the suitability of CAES in areas with high wind penetration (Ibrahim et al., 2010). Several retrofit solutions for existing diesel plants were proposed, where surplus wind energy is used for air compression and subsequently to supercharge diesel generators, leading to significant fuel savings. Similar hybrid configurations were later analyzed by Li et al. (2016) for a small village in the UK, reporting fuel reductions of up to 77%.

More recently, research has increasingly focused on small-scale CAES systems deployed in stand-alone systems and microgrids, with a shift towards configurations in which compressed air is directly converted into electricity via turbines or expanders (Zheng et al., 2025; Fajinmi et al., 2023). For instance, Zhang et al. (2021) investigated a 10 kW CAES system based on scroll machines integrated with wind generation, achieving high renewable energy utilization and a 15.4% reduction in diesel consumption. CAES-based hybrid systems have also been proposed for off-grid telecommunication applications (Zhao et al., 2020). To further improve efficiency, several studies suggest coupling CAES with additional technologies such as Organic Rankine Cycles, hybrid trigeneration systems or desalination units (Ouyang et al., 2022; Alzahrani et al., 2024; Congedo et al., 2022). While these solutions enhance overall performance, they often increase system complexity and rely on auxiliary resources or services (e.g., water demand) that are not always present or justified.

From a methodological perspective, many studies focus on CAES design under nominal conditions, while off-design and partial-load operation are frequently neglected. However, accounting for realistic operating conditions is essential for accurate performance assessment, reliable system sizing, and operational optimization (Rahbari et al., 2021; Arabkoohsar et al., 2020). Due to the strong coupling among system components, CAES systems require integrated design and optimization approaches to avoid efficiency losses and economic penalties, particularly under off-design operation (Heidari et al., 2021; Congedo et al., 2022). Methodologically, existing studies range from parametric analyses to heuristic and evolutionary optimization techniques, which are well suited to highly coupled systems with large design spaces (Mohamad et al., 2019; Bazdar et al., 2022). While advanced optimization methods have been widely applied to utility-scale CAES, their extension to small-scale, off-grid applications remains limited. Recent works demonstrate that optimized CAES sizing and operation can significantly reduce diesel fuel consumption in rural systems, while also highlighting that neglecting off-design behavior leads to overly optimistic performance estimates (Sarmast et al., 2024; Adib et al., 2023); this issue reflects broader optimization challenges commonly encountered in microgrid design beyond CAES applications (Saini and Singal, 2024; He et al., 2023; Dawoud et al., 2018).

Regarding environmental performance, LCA studies on CAES and energy storage systems are growing but remain fewer than techno-economic analyses. In the review of Rahman et al. (2020) over a wide range of 91 analyzed publications, 58 deal with techno-economic aspects and only 33 on life cycle assessment. Reported global warming potential values vary widely (20–740 gCO_2eq/kWh), mainly depending on the electricity mix and storage efficiency. Several studies highlight that operational emissions dominate the life cycle impact, with construction playing a secondary role (Kapila et al., 2019; Oliveira et al., 2015). Comparisons between PV-only and PV–CAES systems indicate that while storage improves self-consumption, it may increase overall environmental impacts (Cocco et al., 2023). Most LCA studies focus on utility-scale applications, whereas small-scale systems remain underexplored. Moreover, environmental benefits are often expressed in terms of avoided emissions rather than through comprehensive cradle-to-grave assessments (Carvalho et al., 2025; Lashgari et al., 2022; Adib et al., 2023). As a result, despite the growing recognition of LCA as a key sustainability assessment tool (Elzein et al., 2019), harmonized and robust environmental assessments of CAES in distributed applications are still lacking (Bazdar et al., 2022).

Overall, the literature reveals several gaps in the assessment of small-scale CAES systems for off-grid applications. Despite growing interest, many studies still rely on simplified or design-point models that do not adequately represent the interactions among renewable generation, storage components, and user demand under time-varying and off-design conditions, limiting the reliability of system sizing and performance evaluation. Environmental assessments are also less developed, particularly for small-scale systems: most LCA studies focus on utility-scale applications, often report avoided emissions, and rarely examine the effects of system scale, configuration, and operational strategy. Moreover, integrated frameworks that jointly address dynamic operation, component sizing, optimization, and environmental performance remain limited for small-scale CAES. Although advanced optimization methods are increasingly used, they are mainly developed for large-scale systems, leading to fragmented techno-economic and environmental assessments and a wide range of reported results. These gaps point to the need for system-oriented methodologies tailored to small-scale CAES in off-grid microgrids, combining realistic operational modeling with techno-economic and environmental evaluation.

1.3. Study objectives, novelties and key contributions

Motivated by the gaps identified in the previous section, this study aims to advance the assessment of small-scale CAES for off-grid applications by quantitatively evaluating the effects of micro-CAES integration in hybrid energy systems. The main objective is to quantify the extent to which the inclusion of micro-CAES can improve environmental performance and cost-effectiveness compared to conventional diesel-only and PV–diesel configurations, under different boundary conditions of solar resource availability, fuel price, and electricity demand.

To support this objective, the following development goals are pursued:

(i) to set up an integrated framework that combines dynamic system modeling, optimization-based component sizing, and cradle-to-grave life cycle assessment, enabling a consistent comparison of alternative system configurations across different locations and boundary conditions;
(ii) to apply the proposed framework to evaluate the sensitivity of techno-economic and environmental performance to system scale, assessing how changes in user demand and component sizing affect the viability of micro-CAES integration.

The main contributions of this work can be summarized as follows:

- A unified optimization-based framework couples dynamic off-design thermodynamic modeling with economic evaluation and life cycle assessment, enabling the simultaneous assessment of performance, costs, and environmental impacts under realistic operating conditions.

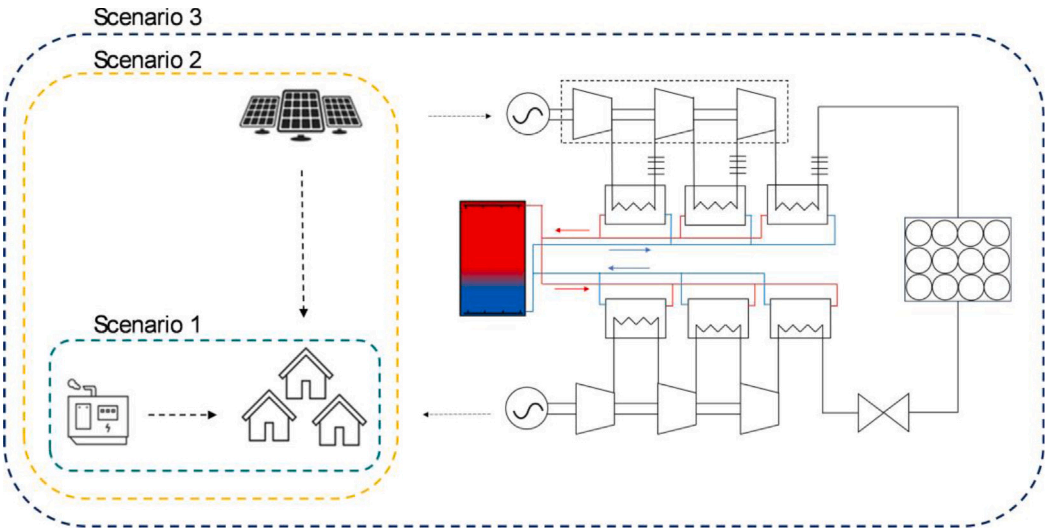

Fig. 1. Schematic diagram of the diesel–PV–CAES system.

- While existing studies predominantly focus on utility-scale CAES installations, this work provides a cradle-to-grave life cycle assessment of micro-CAES integrated into stand-alone hybrid PV–diesel energy systems, based on commercially realistic components and operating constraints relevant to off-grid.
- Component-level parametric life cycle inventories are developed for the main CAES components using market-based size–mass scaling relationships, enabling consistent environmental assessment across different system sizes. The robustness of the proposed framework is evaluated through Monte Carlo analysis, providing confidence intervals for the environmental indicators.
- A comparative analysis of diesel-only, PV–diesel, and PV–diesel–CAES configurations is performed across representative case studies, assessing how geographic location, user scale and diesel fuel price affect environmental and economic performance, and identifying conditions under which micro-CAES integration is beneficial.

Overall, this study contributes quantitative evidence on the role of micro-CAES in off-grid hybrid energy systems and clarifies its potential for reducing greenhouse gas emissions while maintaining economic competitiveness.

The remainder of the paper is organized as follows. Section 2 introduces the modeling framework adopted in this study, describing the hybrid PV–diesel-micro–CAES system and the set of scenarios analyzed. Section 3 presents the overall methodological framework, encompassing the dynamic simulation approach, the optimization-based sizing procedure, and the life cycle assessment methodology, with particular emphasis on the development of the parametric life cycle inventory. Section 4 reports and discusses the techno-economic and environmental results obtained for the different system configurations and case studies. Finally, Section 5 summarizes the main findings, discusses the main limitations of the study, and outlines directions for future research.

2. System description

The analyzed system is a stand-alone energy system comprising an end-user load, a diesel generator, a photovoltaic plant, and an adiabatic micro-CAES unit. The latter is composed of a 3-stage reciprocating compressor, six counterflow heat exchangers, a stratified thermal energy storage system (TES), a series of high-pressure vessels, a throttling valve, and a series of three rotary expanders. The layout is derived from the one analyzed in a previous work of the authors (Tumminello et al., 2024). It is useful to briefly recall that the analyzed system configuration was designed to investigate the use of commercially available components. For this reason, limitations on the maximum compressor discharge temperature and the maximum expander inlet pressure were imposed, specifically 150 °C and 45 bar, reflecting the technological constraints of the machines under consideration (Dumont et al., 2018)

To assess the environmental and economic benefits of hybridization, three operational scenarios are analyzed and compared with the diesel-only baseline:

- Scenario 1: the user load is supplied exclusively by the diesel generator;
- Scenario 2: the PV plant provides electricity whenever solar energy is available, while the diesel generator compensates for the residual demand;
- Scenario 3: the system integrates a CAES unit, which stores surplus PV energy in the form of compressed air and releases it during shortages. The diesel generator operates only as a back-up.

Fig. 1 schematically illustrates the system and the three scenarios.

3. Methodology

3.1. Energy analysis

To perform the energy analysis, the system is modeled within the OpenModelica environment (Fritzson et al., 2005). Each component is represented by a set of differential–algebraic equations describing its functional behavior, including time-dependent effects. Mass and energy balances are imposed for all components. The main governing equations are summarized in Table 1. The following paragraphs provide additional details on the modeling assumptions adopted for the main system components. The compressor is modeled as an adiabatic compression process with subsequent heat dissipation to the ambient. The outlet temperature is limited to a maximum allowable value, and the excess thermal energy with respect to the adiabatic temperature rise is assumed to be fully dissipated to the surroundings. The thermal energy storage system is modeled using a control-volume approach. Due to its stratified configuration, the TES is discretized into a series of lumped control volumes within a one-dimensional framework, with energy balance equations formulated for each volume to capture stratification effects while preserving computational efficiency.

For both the compressor and the expander, the isentropic and volumetric efficiencies are modeled as functions of the pressure ratio and the rotational speed. With specific reference to the expander,

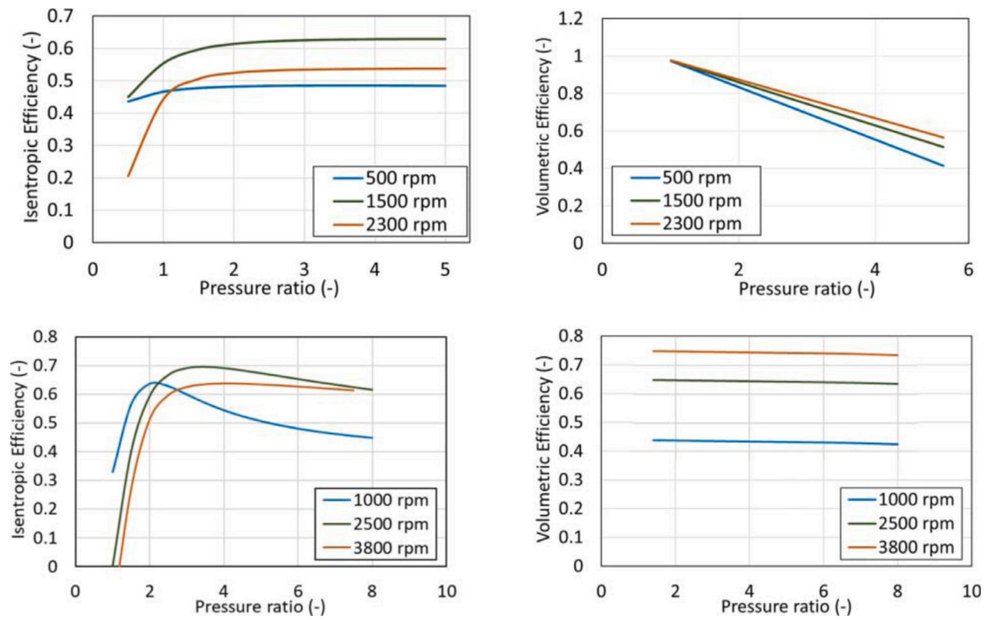

Fig. 2. Compressor and expander efficiency curves as function of pressure ratio and rotational speed.

Table 1
Main equations describing the behavior of CAES components.

Component	Equations
Compressor	$P_c = \dot{m}_{air} \cdot \frac{1}{\eta_{is,c}} \cdot \frac{\gamma}{\gamma-1} \cdot R \cdot T_{in} \cdot \left(\beta^{\frac{\gamma}{\gamma-1}} - 1\right)$ $T_{out} = min(T_{ad}, T_{max})$ $\dot{Q}_{amb} = \dot{m}_{air} \cdot c_p \cdot (T_{out} - T_{ad})$
Expander	$P_{ex} = \dot{m}_{air} \cdot \eta_{is,ex} \cdot \frac{\gamma}{\gamma-1} \cdot R \cdot T_{in} \cdot \left(\frac{1}{\beta}^{\frac{\gamma}{\gamma-1}} - 1\right)$
HEX	$\dot{m} \cdot (h_{in} - h_{out}) = \varepsilon \cdot \dot{Q}_{max}$ $\varepsilon = \frac{1-e^{(-NTU\cdot(1-Cr))}}{1-Cr\cdot e^{(-NTU\cdot(1-Cr))}}$ $NTU = \frac{UA}{C_{min}}$ $\frac{1}{U} = \frac{1}{\alpha_{air,n}}\left(\frac{\dot{m}_{air,n}}{\dot{m}_{air}}\right)^{0.8} + \frac{1}{\alpha_{oil,n}}\left(\frac{\dot{m}_{oil,n}}{\dot{m}_{oil}}\right)^{0.8}$
CAS	$\frac{dU}{dt} = \dot{m}_{in} \cdot h_{in} - \dot{m}_{out} \cdot h_{out} + \dot{Q}_{amb}$
TES	$\rho c_p V_i \frac{dT_i}{dt} = \dot{m}_{in} \cdot h_{in} - \dot{m}_{out} \cdot h_{out} +$ $+ \frac{kA}{l_i}(T_{i+1} - 2T_i + T_{i-1}) - \dot{Q}_{amb}$
Valve	$h_{out} = h_{in}$
PV system	$P_{PV} = P_{PV,p} \cdot \frac{I}{I_{STC}} \cdot PR$
Diesel generator	$P_{DG} = \dot{m}_{fuel} \cdot LHV \cdot \eta_{DG}$

rotary volumetric machines are the most suitable solution for micro- and small-scale applications, with scroll and screw technologies being the most widely adopted. However, screw expanders are generally not recommended for power capacities below 10 kW due to increased leakage losses and manufacturing challenges at reduced scales (He and Wang, 2018), and scroll expanders are therefore typically preferred. Since the present work consists of a parametric analysis in which the expander size may vary over a wide range, a unified efficiency model is adopted as a first-order approximation to represent both scroll and screw expanders. This choice is supported by the comparable operating ranges reported in the literature in terms of built-in volume ratio, pressure ratio, and rotational speed (Dumont et al., 2019; Zhao et al., 2019), as well as by the similar macro-trends observed in their characteristic performance curves. In particular, both technologies exhibit a bell-shaped isentropic efficiency, with reduced efficiency at low pressure ratios due to over-expansion losses and a milder decrease at high pressure ratios associated with under-expansion phenomena. The volumetric efficiency is mainly influenced by the rotational speed and generally decreases as the speed is reduced. While quantitative differences may exist, these are strongly case-dependent and do not affect the overall performance trends (Dumont et al., 2018; Giuffrida, 2017; Braimakis et al., 2025; Zhang et al., 2017). Additional support for this modeling approach is provided by Dumont et al. (2018), who showed that the predicted optimal isentropic efficiency curves of scroll and screw expanders are very close, while larger deviations occur for piston and roots machines. The performance maps are therefore generated using the parametric formulation proposed by Declaye et al. (2013), with parameters derived from the corresponding reference. A maximum isentropic efficiency of 70% is assumed, representative of an average commercial expander, and is not expected to influence the qualitative trends of the results while providing a realistic estimation.

Regarding the compressor, the isentropic efficiency is modeled using the same functional form adopted for the expander, with coefficients modified through a fitting procedure based on in-house experimental data, whereas the volumetric efficiency trends are derived from (Lyons and Plisga, 2011). Fig. 2 shows the isentropic and volumetric efficiency maps adopted for the compressor and the expander.

3.1.1. Operational strategy of the hybrid system

The system operation is governed by an energy management strategy designed to ensure instantaneous power balance while prioritizing renewable energy sources. Depending on the considered configuration, the electrical load may be supplied exclusively by diesel generation, by a combination of diesel and photovoltaic power, or by diesel, photovoltaic generation, and CAES. Priority is always assigned to renewable sources, namely photovoltaic generation and the CAES unit. Consequently, the diesel generator is dispatched only when these sources are insufficient to meet the load demand, thereby acting as a back-up unit to ensure system reliability. More specifically:

- In Scenario 1, the load is supplied exclusively by the diesel generator. Accordingly, the diesel generator power is defined as follows:

$$P_{DG}(t) = P_L(t) \tag{1}$$

  where $P_{DG}(t)$ is the power generated by the diesel while $P_L(t)$ is the power instantly requested by the load.
- In Scenario 2, the photovoltaic generation is directly used to meet the load whenever available, while the diesel generator compensates for the residual demand.

$$P_{DG}(t) = \max\{0,\ P_L(t) - P_{PV}(t)\}. \tag{2}$$

- In Scenario 3, photovoltaic power is first allocated to the load, and surplus is then directed to the CAES system. Defining $\Delta P(t)$ as the power imbalance between the photovoltaic production and user demand

$$\Delta P(t) = P_{\mathrm{PV}}(t) - P_L(t). \tag{3}$$

When $\Delta P(t)$ is greater than the minimum power required to operate the compressor at the minimum admissible rotational speed and the storage pressure inside the pressure vessel is below the maximum limit p_{max}, the CAES operates in charging mode. The compressor absorbs a power equal to the minimum between the available power surplus and the maximum admissible compressor power at maximum rotational speed, consistently with the instantaneous stages pressure ratios:

$$P_{\mathrm{c}}(t) = \min\left[\Delta P(t),\ P_{\mathrm{c,max}}\right]. \tag{4}$$

Conversely, when photovoltaic generation is insufficient to meet the load ($\Delta P(t) < 0$) and the storage pressure exceeds the minimum threshold p_{min}, the CAES operates in discharging mode, delivering

$$P_{\mathrm{ex}}(t) = \min\left[\max\left(-\Delta P(t),\ P_{\mathrm{ex,min}}\right),\ P_{\mathrm{ex,max}}\right]. \tag{5}$$

where minimum deliverable power $P_{ex,min}$ corresponds to the operation of the expander at its minimum rotational speed N_{min}. Similarly, the maximum power output allowed by the expander characteristics is indicated as $P_{ex,max}$. If neither condition is satisfied, the CAES remains idle. The diesel generator is used to close the overall system power balance when the combined power provided by the PV and CAES units is insufficient to meet the load demand. Accordingly, the power supplied by the diesel generator is defined as:

$$P_{\mathrm{DG}}(t) = \max\left\{0,\ P_L(t) - P_{\mathrm{PV}}(t) - P_{\mathrm{ex}}(t)\right\}. \tag{6}$$

By construction of the energy balance, all scenarios are designed to supply the same electrical load profile. Unmet demand is assumed to be zero and is fully compensated by the diesel generator operation.

3.1.2. Energy key performance indicator

Energy performance is evaluated through the Round-Trip Efficiency (RTE) and the Renewable Self-Sufficiency (RSS), defined in Eq. (7) and Eq. (8), respectively. The round-trip efficiency is defined as the ratio between the energy released by the expander and the energy absorbed by the compressor, providing an indication of the effectiveness of the energy storage and conversion process. The renewable self-sufficiency represents the ratio between the total energy supplied by the CAES system and the photovoltaic generator and the total energy demand of the user load (E_L), quantifying the degree to which the user demand can be covered by locally generated and stored renewable energy. Both performance indicators are evaluated over an annual time horizon. To reduce computational effort, system operation is approximated using four representative weeks corresponding to different seasons, simulated sequentially with a global cyclic constraint on the storage pressure to ensure consistency with annual operation.

$$RTE = \frac{E_{ex}}{E_c} \tag{7}$$

$$RSS = \frac{E_{PV} + E_{ex}}{E_L} \tag{8}$$

3.2. Economic analysis

The economic analysis is based on the evaluation of the system Levelized Cost of Energy. Eq. (9) defines the LCOE as a function of the total capital expenditure (CAPEX), the annual costs (AC), and the total annual electrical energy delivered to the end user by all energy sources (E_L). The annual costs include maintenance cost as well as diesel fuel purchase costs. Both the annual costs and the annual electrical energy delivered to the end user are assumed to remain constant over the system lifetime. The investment cost of each system component is estimated using the cost functions summarized in Table 2 and updated to 2024 values using the Chemical Engineering Plant Cost Index (CEPCI), as expressed in Eq. (10). A system lifetime of 25 years is assumed. Annual maintenance costs are taken as 2% of the total capital investment, and a discount rate of 0.05 is adopted, in line with values commonly used in techno-economic assessments of similar energy systems (Wu et al., 2020; Li and Duan, 2023; Cioni et al., 2023).

$$LCOE = \frac{CAPEX + \sum_{i=1}^{Y} \frac{AC}{(1+d)^i}}{\sum_{i=1}^{Y} \frac{E_L}{(1+d)^i}} \tag{9}$$

$$C_{actual} = C_{ref} \cdot \frac{CEPCI_{actual}}{CEPCI_{ref}} \tag{10}$$

3.3. Life cycle assessment

The environmental analysis is based on the Life Cycle Assessment methodology, as standardized by ISO 14040 and ISO 14044 (International Organization for Standardization, 2006; Standard, 2006). In accordance with the methodological framework of LCA the goal and scope of the analysis are first defined. The scope of the study, as extensively described in the Introduction and in Section 2, focuses on small-scale CAES. The goal of the LCA is to develop a parametric life cycle inventory (pLCI) model aimed at quantifying the environmental impacts associated with micro-CAES systems. Within a broader system-level perspective, this model enables the inclusion of environmental performance indicators, especially climate change, as optimization criteria in the overall energy system model.

The adopted methodological approach is based on a cradle-to-grave perspective for each process included within the system boundaries. Accordingly, the construction phase, the operation and maintenance phase, and the end-of-life are taken into account. The system boundaries encompass all components involved in the energy storage system as well as the energy generation units. The transportation of components to the site, the elements of the electrical transmission network supplying end users, the piping system, and control devices are excluded from the analysis. Fig. 3 provides a detailed representation of the system boundaries.

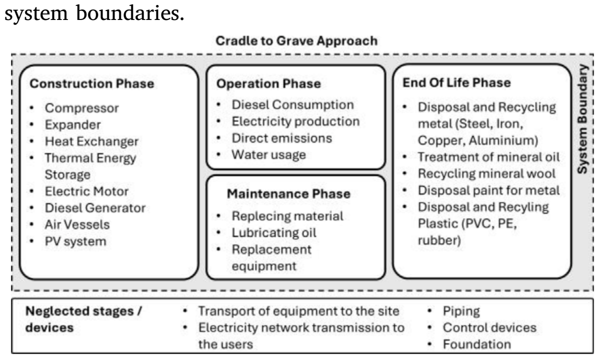

Fig. 3. System Boundary for the LCA analysis.

The functional unit for the analysis is 1 kWh of electrical energy supplied to the end user. Life cycle impacts are calculated considering the entire system lifetime of 25 years and are normalized by the total electrical energy delivered over the lifetime. For the analysis,

Table 2
Cost function for main system components.

Component	Capital cost estimation [$]	Year	CEPCI	
Compressor	$C = 13000 \cdot (\frac{P\,(\mathrm{kW})}{8})^{0.61}$	2016	541.7	Couper (2005)
Expander	$C = 1810 \cdot P\,(\mathrm{kW})^{0.71}$	2005	468.5	Couper (2005)
Heat exchanger	$C = 1096 \cdot \left(10.76 \cdot A\,(\mathrm{m}^2)\right)^{0.18}$	2005	468.5	Couper (2005)
Air reservoir	$C = 1000 \cdot V\,(\mathrm{m}^3) \cdot F_p$	2022	816	Cheayb et al. (2022)
	$F_p = \frac{1}{0.0063} \cdot (\frac{(p_{\max}\,(\mathrm{bar})+1)\cdot D}{2(850-0.6(p_{\max}+1))} + 0.00315)$			
Thermal oil tank	$C = 423 \cdot V\,(\mathrm{m}^3)$	2018	605.2	Xue and White (2018)
Thermal oil	$C = 2.7 \cdot m\,(\mathrm{kg})$	2018	605.2	Wu et al. (2020)
PV system	$C = 1050 \cdot P_p\,(\mathrm{kW}_p)$	2023	803.3	Lazard (2023)
Diesel generator	$C = 630 \cdot P\,(\mathrm{kW})$	2017	567	Gnana (2017)
Motor/Generator	$C = 60 \cdot P\,(\mathrm{kW})^{0.92}$	2022	816	Li et al. (2022)

the Ecoinvent 3.10 database (Ecoinvent, 2023) and the OpenLCA software (Openlca, 2025) were employed. The environmental impacts are computed through the Environmental Footprint 3.1 methodology. In particular, to facilitate the optimization process where the size of CAES equipment is changed, directly affecting the environmental impact, emphasis was put on generating a pLCI. The creation of a pLCI consists of two main steps:

- Finding a reliable reference in order to construct an LCI of the considered component;
- Finding enough data to establish a relationship between the inventory and the size of the components.

This translates into relating the size of a component to a characteristic parameter (so-called life cycle parameter) and parameterizing the inventory in terms of it. In this work, the life cycle parameter is the mass for all the equipment, except for the PV installation; for the latter the installed peak power is considered. Firstly, an extensive market research has been conducted for each component; subsequently, one or more regressions were derived using a least squares methodology. The type of regression (i.e. linear, quadratic, power or logarithmic) was selected based on which model exhibited the highest coefficient of determination (R^2). The obtained equations represent the relationship between mass and the scale of the components. The reference LCI, collected for a specific size, is then scaled according to these correlations. All the reference LCI are available in the Supplementary Material of this manuscript. The scaled LCI describe materials and energy required and can be then converted into environmental impact following the LCA procedure. Specifically, the parameters that describe the size of the components are: power for compressor, expander, electric motor and diesel generator; volume capacity for the thermal energy storage; nominal heat power for heat exchangers; kW of peak power for PV plant and both volume capacity and allowable pressure for air reservoir, for the last two components a slightly different approach is followed as described later on.

To estimate the uncertainty introduced by the use of these correlations in the calculation of the environmental impact, a Monte Carlo analysis is performed. In this analysis, the total mass of each component is randomly varied within a specific uncertainty range, for a total of 10,000 calculations. Specifically, a Gaussian distribution is assumed around the correlation, with a standard deviation equal to the root mean square error (RMSE) of the regression, as described in Eq. (11). In this formulation, given a pair size–mass (x_i, y_i) derived from the market, $f(x_i)$ denotes the corresponding mass approximation provided by the regression. The Monte Carlo analysis provides, as final results, both the mean value of the impact indicator and the 95% probability confidence interval. This approach is commonly adopted for uncertainty quantification in life cycle assessment studies (Raynolds et al., 1999; Kabir et al., 2012). The uncertainty evaluation is carried out only for the configurations resulting from the optimization process. During this process, the mass is directly computed through the proposed correlations. Moreover, the uncertainty analysis accounts exclusively for the uncertainty associated with the overall mass estimation based on the parametric inventory, and does not include other potential sources of uncertainty in the LCA (e.g., allocation of mass to different materials, characterization factors, etc.).

$$\sigma = RMSE = \sqrt{\frac{1}{N}\sum_{i=1}^{n}(f(x_i) - y_i)^2} \quad (11)$$

3.3.1. Compressor

The market analysis focused on reciprocating air compressors with multiple compression stages (typically 3–4) and operating pressures ranging from 50 to 200 bar. A broad power range was considered, extending to the upper applicability limits of this technology (~1MW). Fig. 4 reports the market data together with the correlation derived from them and 95% confidence interval $[-1.96\sigma, 1.96\sigma]$ of the associated gaussian distribution. A total of 238 products are considered derived from 10 of the most important compressor manufacturers (Boge, Atlas Copco, Dream Compressor, Denair, Burckardt, Sauer, Blaskmer, Sunceter, Bauer) (Boge, 2025; Atlas Copco, 2025; Dream Compressor, 2025; Denair, 2025; Burckardt, 2025; Sauer compressors, 2025; Blaskmer, 2025; Sunceter, 2025; Bauer compressors, 2025). Due to the scarcity of reliable data in the open literature, the LCI of an internal combustion engine was adopted as a reference, specifically the Ecoinvent dataset "*Internal combustion engine production, passenger car*". This choice is motivated by the substantial equivalence of the two devices in terms of material composition and operating principle. Both systems share the same modular structure, consisting of pistons, cylinders, valves, a crankshaft, and a housing. Consequently, their manufacturing processes can be considered analogous.

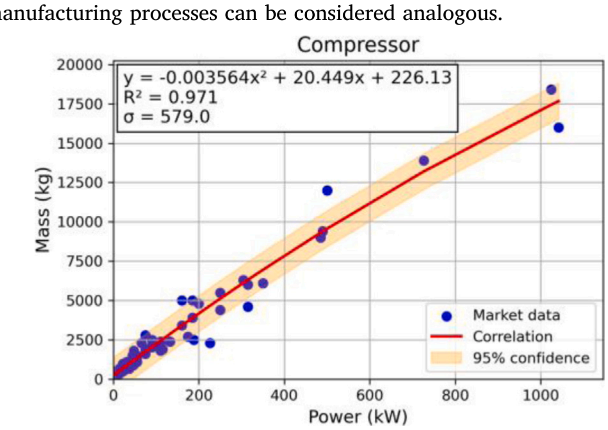

Fig. 4. Compressor power - mass correlation.

3.3.2. Expander

As described in Section 3.1, the expander model can represent both scroll and screw expanders, with the transition from one technology to the other depending on the machine size. From an environmental assessment perspective, the market analysis was carried out for both categories. However, due to the lack of available data concerning both inventory parameters and mass-to-power ratios, scroll and screw

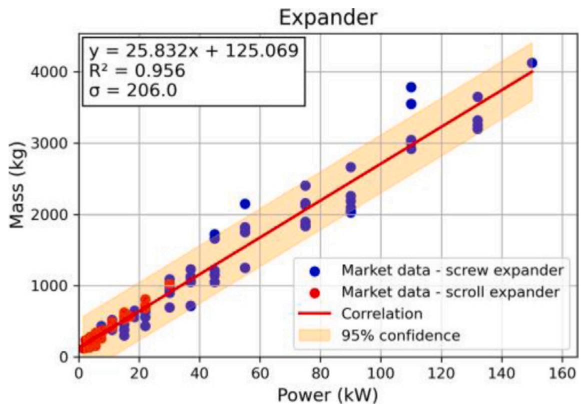

Fig. 5. Expander power - mass correlation.

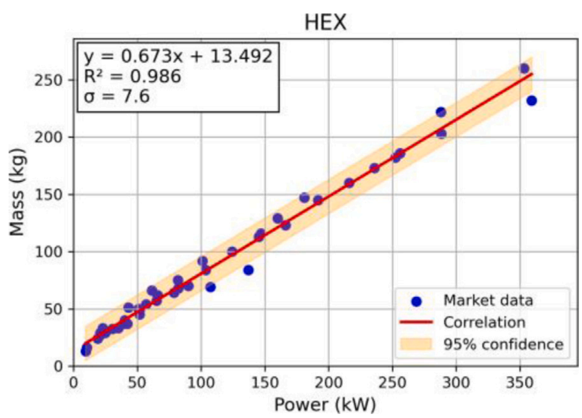

Fig. 6. Heat exchanger power - mass correlation.

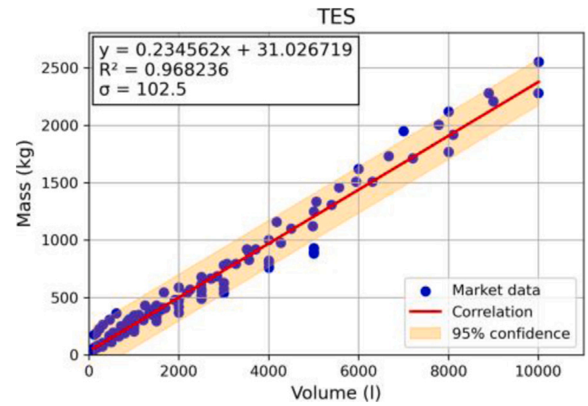

Fig. 7. TES volume - mass correlation.

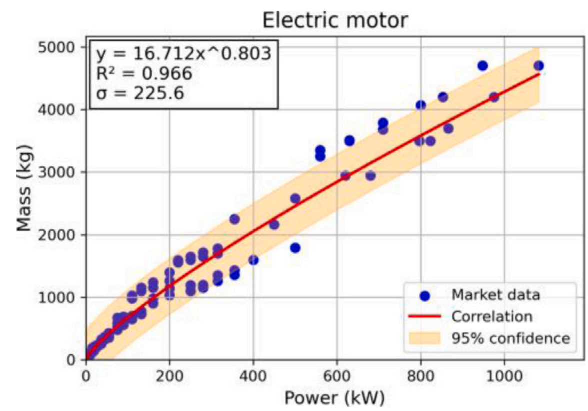

Fig. 8. Electric motor power - mass correlation.

expanders have been treated as compressors. Mass data are retrieved from catalogs of Atlas Copco and Fini Compressor for scroll compressor (Atlas Copco, 2025; Fini compressors, 2024) and Denair, Elang and Kaishan Compressor (Denair, 2025; Ielang, 2025; Kaishan USA, 2025) for screw compressor. As shown in Fig. 5, a single correlation can be defined that effectively approximates the mass of both machine types. Furthermore, manufacturer datasheets include not only the compressor itself but also the skid, the electric motor, and junction elements, further reducing the differences between the two technologies. For this reason, it was considered reasonable to assume their equivalence also in the impact assessment phase. The Ecoinvent process "*4 kW screw compressor*" has been chosen as the reference.

3.3.3. Heat exchanger

Regarding the heat exchanger, since the system operates at high pressures, only data referring to steel components have been considered, data are derived from Pilan and Bowman catalogs (Pilan, 2025; Bowman, 2025). The nominal heat transfer rate was selected as the characteristic sizing parameter, as it provides a more robust correlation compared to a correlation based on heat transfer surface. Heat exchangers with the same surface but different mass flow rates, and consequently different tube diameters, exhibit significantly different masses. Fig. 6 shows the correlation obtained. The reference LCI was taken from the work of Cioccolanti et al. (2019), which describes a shell-and-tube heat exchanger employed in a micro-ORC system.

3.3.4. Thermal energy storage

To establish a volume–mass correlation for thermal energy storage, the market analysis focused on hot water storage tanks, as substantially more data are available for this product and the storage medium does not affect the results. In the Supplementary Material, "Appendix C: Thermal Energy Storage Selection", a more detailed justification is provided, including a comparison of processes available in the Ecoinvent database. Market data were collected from the catalogs of ADCA Therm, IES, McKenna, Unical, Ekin, Tanpera, Kodsan, and AOSmith (Valsteam ADCA, 2025; I.E.S. Group, 2025; McKenna Boiler, 2025; Unical, 2025; Endüstriyel, 2025; Kodsan, 2025; Smith, 2025). The resulting correlation is reported in Fig. 7. For TES production modeling, a 270 L hot water tank, representative of small-scale solar thermal plants, was selected as reference. The LCI was derived from the work of Greening and Azapagic (2014). The storage medium was modeled separately, using the Ecoinvent dataset "lubricating oil" and assessing its environmental impact directly based on its total mass.

3.3.5. Electric motor

While the reference inventory for expanders already includes the electric machine, in the case of compressors it was necessary to identify a suitable reference and develop a dedicated correlation, treating the motor as a separate component. Data were retrieved from Orange and OMEC website (Orange1, 2025; Omec, 2025), considering only motors with efficiency class IE3 and a cast iron body, to ensure consistency with the selected reference case (Cassoret et al., 2019), Fig. 8 displays the market data and the derived correlation. The same power range explored for compressors was adopted for the motors. Although modeled independently, in the results section the impact for the electric motor are presented together with those of the compressor it drives, following the same approach applied to expanders.

3.3.6. Diesel generator

For diesel generators, a single regression is not sufficient to properly fit the market data. Therefore, the power range was divided into two

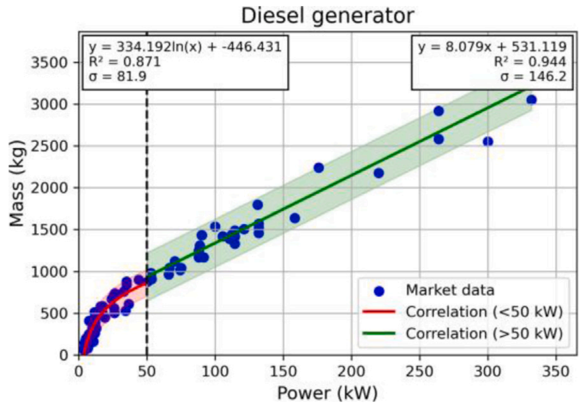

Fig. 9. Diesel generator power - mass correlation.

domains, with a threshold at 50 kW. As shown in Fig. 9, a logarithmic regression is applied for units below 50 kW, while a linear regression for higher powers. Although the two correlations are not continuous at the division point, the discrepancy between them is below 7%, which is acceptable for the purposes of this analysis. Market data are collected from the catalogs of Green Power Generators, Pramac, Yanmar, and CRI Fluid (Green power generators, 2025; Pramac, 2025; Yanmar, 2025; CRI, 2025). The reference LCI is based on a 5 kW diesel generator with a mass of 112 kg described in the study of Alsema (2000). The contributions from diesel generator use phase are estimated using the relevant Ecoinvent processes: *"Machine operation, diesel, < 18.64 kW, generators", "Machine operation, diesel, ≥ 18.64 kW and ≤ 74.57 kW, generators", and "Machine operation, diesel, > 74.57 kW, generators"*, according to the generator's nominal power. The inventories of these processes are scaled using the mass of diesel consumed as the scaling parameter. The diesel consumption (in kilograms) is calculated assuming a lower heating value (LHV) of 42,680 kJ/kg and an average generator efficiency of 0.35. The diesel generator experiences efficiency variations under off-design operating conditions. Nevertheless, preliminary analyses indicate that adopting a constant efficiency assumption results in negligible variations in the overall system performance indicators and does not affect the conclusions of the study. Accordingly, a constant average efficiency is assumed in this work in order to simplify the model.

3.3.7. Air vessels

For the air reservoir, no market-based correlation is introduced, but a different approach is adopted in order to explicitly capture the influence of both volume and maximum pressure on material demand. Vessel sizing is therefore carried out following the method proposed by Liu et al. (2014) and summarized in Eq. (12)–(14). In these equations, δ denotes the vessel wall thickness, while σ_{allow} is the allowable tensile stress defined as $\sigma_{\text{allow}} = \sigma_y / SF$, with σ_y the yield strength. The considered reservoirs are standard 50 L steel bottles with an aspect ratio of 6. The selected material is 30CrMoE steel (density 7850 kg m^{-3}, yield strength 835 MPa), and a safety factor of 2.5 is applied. The resulting material demand, and thus the environmental impact, depends on both storage volume and maximum pressure, both key parameters in CAES performance and optimization. The reference inventory for compressed air reservoir is derived from the study of Joshi (2017). The ecoinvent database provides three main categories for steel materials, namely unalloyed steel, low-alloyed steel, and chromium steel. For Air Vessels, the specific steel grade 30CrMoE was modeled using the low-alloyed steel dataset. This choice is justified by its chemical composition, which includes chromium and molybdenum contents exceeding the threshold for unalloyed steels, while remaining well below the levels required for classification as chromium or stainless steel.

$$\delta = \frac{D}{2} \cdot \left(1 - \sqrt{\frac{\sigma_{all} - 1.3 \cdot p_{max}}{\sigma_{all} + 0.4 \cdot p_{max}}} \right) \tag{12}$$

$$V = \frac{\pi}{4} \cdot (D - 2\delta)^2 \cdot AR \cdot D + \frac{\pi}{6} \cdot (D - 2\delta)^3 \tag{13}$$

$$m = \rho \cdot \left(\pi \cdot \delta \cdot (D - \delta) \cdot AR \cdot D + \frac{\pi}{6} \cdot \left(D^3 - (D - 2\delta) \right)^3 \right) \tag{14}$$

3.3.8. PV system

To evaluate the environmental impact of the photovoltaic system, the Ecoinvent process "*Photovoltaic plant construction, 570 kWp, multi-Si, on open ground – GLO*" is selected as the reference. In line with the other components, the PV inventory was scaled during the optimization process, as its size is a key parameter in the analysis. However, unlike for the other components, the design and the life cycle parameters correspond for the PV, thus making the development of a specific correlation not necessary.

3.4. Optimization method

A component sizing optimization procedure is carried out by coupling the thermodynamic model with the Dakota toolkit (Adams et al., 2020). The followed procedure is analogous to that proposed in a previous article by the authors (Tumminello et al., 2024) and it is based on the use of the Efficient Global Optimization (EGO) algorithm (Jones et al., 1998). The optimization relies on a Gaussian Process (GP) surrogate model, which is iteratively updated by selecting new sampling points that maximize the Expected Improvement (EI) of the objective function. The convergence criterion is defined based on the value of the Expected Improvement or on a maximum number of iterations. Since the EI is a dimensional quantity, the convergence threshold is defined with respect to the expected order of magnitude of the objective function. Specifically, convergence is reached when the EI falls below 10^{-3} times the expected order of magnitude of the objective function. The maximum number of iterations allowed for the EGO procedure is set to 100; the maximum number of iterations was selected to ensure convergence in the worst-case scenarios.

The independent variables considered in the optimization procedure include those listed in Table 3, and therefore comprise at least one sizing parameter for each of the main system components, with the exception of the thermal storage unit. The bounds of the design space reported in the table refer to the base-case configuration. As discussed in more detail in the following subsection, in some scenarios the system is scaled to account for increased user demand; in such cases, the corresponding design-space limits are scaled accordingly.

The amount of thermal oil associated with each configuration is calculated as the mass required to guarantee the necessary heat exchange in the case where the air tanks are fully charged from empty (or fully discharged from full), ensuring an oil mass flow rate equal to 0.55 times the air mass flow rate through the heat exchangers. This value is selected to maintain a thermal-capacity ratio close to unity, thereby maximizing the efficiency of thermal recovery.

Concerning the objective function, the optimization was carried out from both economic and environmental perspectives. Three parameters were considered in the study:

- the GWP
- the Single Score indicator (calculated according to the EF methodology)
- the Levelized Cost of Energy

The optimization procedure was applied to both Scenario 2 and Scenario 3. While Scenario 1 offers no room for improvement, as the user demand is fully supplied by the diesel generator, Scenarios

Table 3
Decision variables and bounds for the sizing optimization of the PV–CAES-diesel system (base case)

Parameter	Symbol	Range
Compressor swept volume	$V_{s,c}$	500–4000 cm^3
Expander swept volume	$V_{s,ex}$	10–60 cm^3
Pressure vessels volume	V	10–50 m^3
Max air pressure inside vessels	p_{max}	40–200 bar
PV installed peak power	$P_{PV,p}$	30–200 kW

2 and 3 allow for an optimization process aimed at minimizing either environmental impact or cost. For a given user energy demand, the power supply can be provided through a combination of photovoltaic generation, CAES, and the diesel generator. Adjusting the system configuration through the sizing of individual components, thereby influencing system efficiency, environmental impact, cost, and the relative contribution of each energy source during operation.

3.5. User load demand and system location

The end-user is assumed to be a small residential energy community (e.g., a village). Therefore, the load profile considered corresponds to a statistical average of domestic electricity consumption (Joshi, 2017). As shown in Fig. 10, the load exhibits typical household demand patterns, with two daily peaks occurring in the morning and evening hours. The load is expressed in terms of maximum power demand. In the base case, the peak load is assumed to be 11 kW, corresponding to a total daily consumption of 200 kWh. As detailed in the following sections, in specific scenarios the maximum load is increased in order to assess the impact of system scaling, with analyses carried out up to 3 MWh of daily energy demand. For completeness, the load profile is provided in tabular form in the Supplementary Materials.

To assess CAES performance and the potential economic and environmental benefits, seven different locations have been identified, all situated in countries where the adoption of ESS can support the electrification of rural areas and renewable energy integration. The criteria for selecting the case-study locations are based on three factors: the presence of off-grid areas that could benefit from such a system, the photovoltaic (PV) potential, and the diesel cost. In particular, both PV potential and diesel cost are classified into three ranges (low, medium, and high), and one representative nation is selected for each possible combination. The only exception is the case of low PV potential: here, only a nation with high diesel cost is considered, since it is unlikely that the hybrid system would be advantageous under conditions of both low PV potential and low diesel prices. Based on these considerations, the chosen locations are: Jordan, Cambodia, India, Botswana, Belize, Romania and Zimbabwe. To consider the impact of different climate zones (e.g. temperature) on the efficiency of photovoltaic panels, different values of photovoltaic performance ratio (PR) are considered based on the location, both photovoltaic potential and PR value are derived from Kawajiri et al. (2011), diesel prices are obtained from the "Global Petrol prices" website (GlobalPetrolPrices, 2025). Table 4 summarizes the characteristics of each installation. Hereafter, sites are designated using an acronym that reflects both the photovoltaic potential and the diesel fuel cost. The notation follows a qualitative classification, where H, M, and L denote High, Medium, and Low levels, respectively, while PV refers to photovoltaic potential and C to diesel cost. For instance, Jordan is denoted as HPV–LC (High Photovoltaic potential – Low Cost), the complete list of site acronyms and their corresponding locations is reported in Table 4.

4. Results and discussion

In this section, the results of the study are presented. First, the three scenarios are compared for each location, in terms of environmental aspects. For the sake of brevity, only the results of one of the six studied installations are reported in detail, specifically the one with the lowest greenhouse gas emissions. The outcomes of the other case studies are summarized concisely. For the lower-GWP scenario a comparison with the outcomes obtained when the objective function is expressed in terms of single-score assessment is also presented. Finally, the economic results are described.

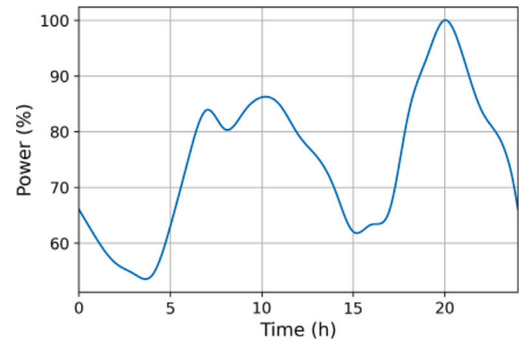

Fig. 10. End-user power demand profile.

Table 4
Characteristics of the analyzed sites.

Location	PV potential [kWh/kW]	PR [–]	Diesel cost [$/l]	Acronym
Romania	1000–1200	0.75	1.609	LPV-HC
Cambodia	1200–1400	0.70	0.942	MPV-LC
India	1200–1400	0.75	1.033	MPV-MC
Belize	1200–1400	0.70	1.486	MPV-HC
Jordan	1400–1600	0.75	0.905	HPV-LC
Botswana	1400–1600	0.75	1.167	HPV-MC
Zimbabwe	1400–1600	0.75	1.55	HPV-HC

4.1. Comparison of different scenarios under GWP minimization

For each case location, the configuration with the lowest greenhouse gas emissions is obtained, for both scenario 2 and 3, using the algorithm described in Section 3.4. Fig. 11 shows the results obtained in terms of equivalent CO_2 emission per kWh, with a focus on the third scenario. Scenario 1, identical across all locations, results in

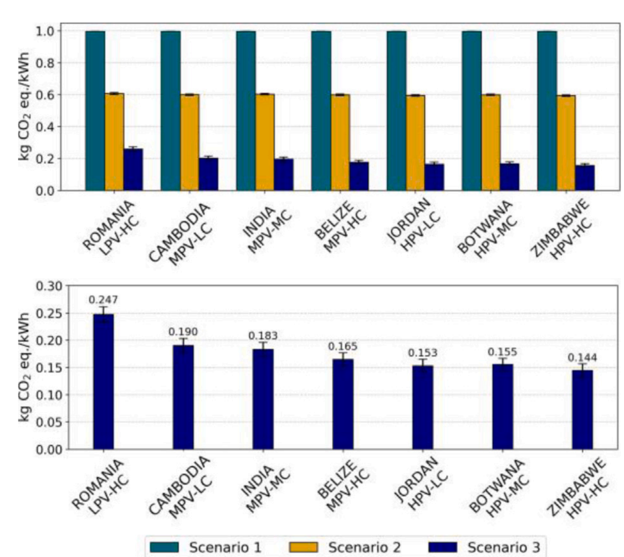

Fig. 11. Global warming potential for the three scenarios.

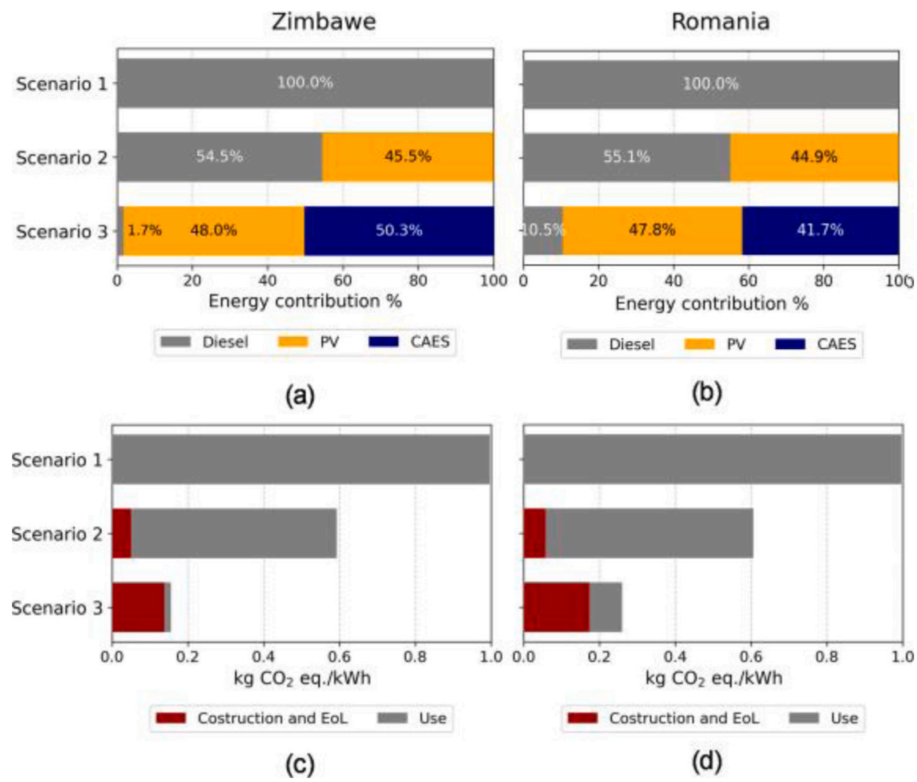

Fig. 12. Energy contribution and GWP breakdown for the three scenarios at the HPV-HC (High Photovoltaic potential – High Cost) and LPV-HC (Low Photovoltaic potential – Low Cost) site.

Table 5
Minimum GWP configuration for Zimbabwe and Romania.

		$V_{s,c}$ [cm^3]	$V_{s,ex}$ [cm^3]	p_{max} [bar]	V [m^3]	$P_{PV,p}$ [kW$_p$]	RSS [%]	RTE [%]
Zimbabwe	Scenario 2	–	–	–	–	38	45.5	–
	Scenario 3	2150	17	91	23.1	74	98.3	35.7
Romania	Scenario 2	–	–	–	–	43	44.9	–
	Scenario 3	2365	19	103	18.4	89	89.5	34.5

0.996 kg CO_2eq/kWh. The addition of a PV system reduces emissions to approximately 0.598 kg CO_2eq/kWh, while implementing CAES in Scenario 3 further lowers emissions by roughly 30%, ranging from 0.144 to 0.247 kg CO_2eq/kWh depending on location. Fig. 12 illustrates the share of energy supplied by diesel, PV, and CAES, along with CO_2eq emissions separated into use and end-of-life (EoL) and construction phases, for the sites with the highest (Romania) and lowest (Zimbabwe) emissions. These results indicate that the reduction in emissions from Scenario 1 to Scenario 3 is primarily due to the decrease in direct diesel generator operation. In Zimbabwe, for instance, the diesel contribution to total energy supply decreases from 100% in Scenario 1, to 54.5% in Scenario 2, and further down to only 1.7% in Scenario 3. Although higher system complexity increases construction-related emissions, as illustrated in Fig. 12(b), the sharp decline in operational emissions ultimately results in lower overall CO_2eq emissions. By comparing the results reported in the graphs for the two locations and the optimal configuration sizing in Table 5, it becomes clear why Scenario 2 exhibits only minor geographical variation, whereas the configuration including CAES shows more pronounced differences. The two sites have markedly different photovoltaic potentials: the LPV site requires a larger PV capacity, and while this difference remains moderate in Scenario 2, it becomes substantial in Scenario 3, where surplus solar energy is stored in the CAES. Under low-PV conditions, renewable coverage remains lower despite a larger installed PV capacity, increasing both construction and operation related impacts. This underscores the central role of the PV system in shaping overall environmental performance, as further discussed in the following sections. For completeness, the full set of results for the seven locations is provided in the Supplementary Material.

The bar charts in Fig. 11 also report the uncertainty associated with the adopted pLCI method, quantified as described in Section 3.3. For the first two scenarios, uncertainty is negligible because impacts are dominated by fuel combustion. In Scenario 3, where construction and end-of-life processes account for most GWP emissions, uncertainty is higher but remains within an acceptable range (±3.5% of the total). Furthermore, Table 5 reports a round-trip efficiency of approximately 35%. Although relatively low, this value is consistent with documented performance of micro-CAES systems based on conventional technologies, which do not employ advanced concepts such as isothermal machines still under development (Zheng et al., 2025). The use of reciprocating compressors and volumetric expanders, characterized by modest efficiencies and significant thermal losses, largely explains this outcome. As a consequence, the low RTE necessitates a substantial oversizing of the PV array, which increases markedly when transitioning from the PV–Diesel to the PV–Diesel–CAES configuration and, as will be shown, constitutes a major contributor to the overall environmental burden of the system.

To further compare the environmental impact of the three different scenarios, Fig. 13 reports the absolute value of four relevant impact indicators at the midpoint-level in the three scenarios, while Fig. 14

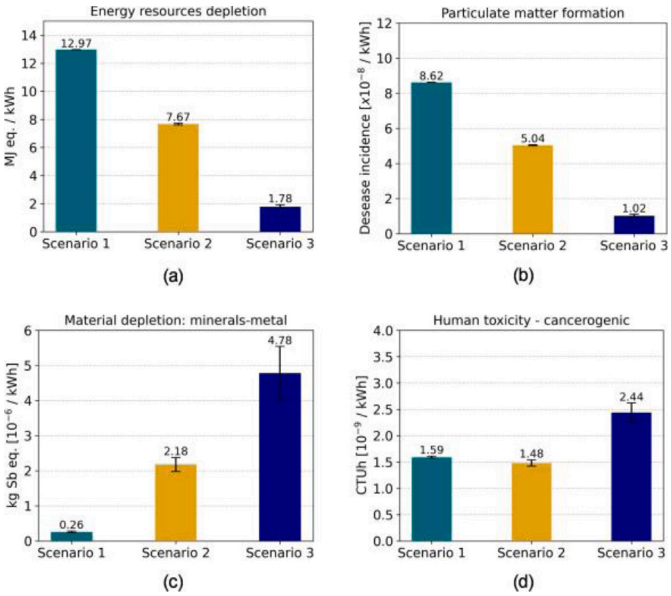

Fig. 13. Comparison of relevant midpoint for the three scenarios at the HPV-HC site: (a) Energy resource depletion - (b) Particulate matter formation - (c) Material depletion - (d) Human toxicity carcinogenic.

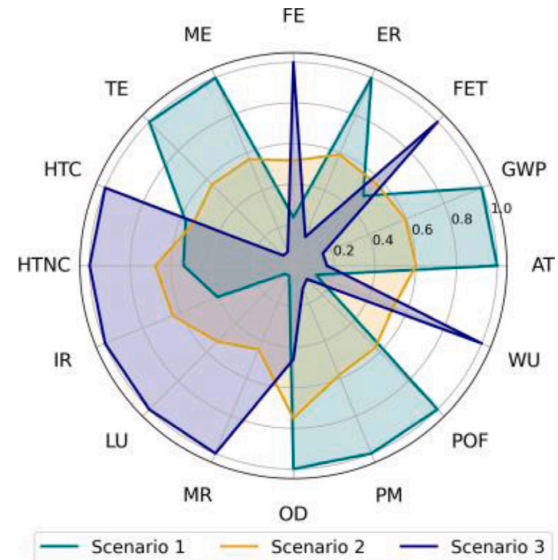

Fig. 14. Midpoint comparison for the three scenarios at the HPV-HC site.

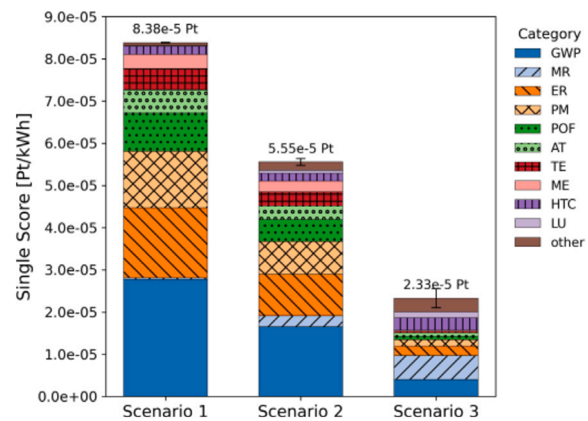

Fig. 15. Comparison of single score for the three scenarios at the HPV-HC Site.

shows the value of all the midpoint indicators normalized over the maximum. Fig. 13a–b highlight the categories energy resource depletion (ER) and particulate matter formation (PM), which decrease by about 40% from Scenario 1 to Scenario 2. In Scenario 3, reductions are even more pronounced, reaching 86% and 88%, respectively. These improvements are mainly due to the sharp decrease in diesel use; although non-renewable energy demand increases during construction, diesel consumption during operation remains the dominant factor. Conversely, Fig. 13c–d show opposite trends. Mineral resource depletion (MR) rises steadily from Scenario 1 to Scenario 3 as system components increase, while human toxicity - carcinogenic (HTC) remains nearly unchanged between Scenarios 1 and 2 but almost doubles in Scenario 3. This effect is linked to metal processing, as steelmaking in electric arc or basic oxygen furnaces generates large amounts of toxic slag requiring treatment and disposal. Once again, the uncertainty introduced by the proposed correlations leads to negligible values in the first two scenarios. In the third scenario, it remains negligible for the categories where the impact is associated with combustion (i.e. energy resource depletion and particulate matter formation), while it becomes more relevant for while human toxicity carcinogenic and mineral resource depletion . In particular, the uncertainty increases significantly for the MR category, which is more closely related to the mass of individual components. In this case, for Scenario 3, the uncertainty reaches approximately ±15%, indicating that the estimation cannot be considered fully reliable. Nonetheless, such elevated uncertainty values are observed exclusively for this category and in this specific scenario. A more precise estimation would be required for a detailed assessment of this category; however, overall, the estimated impacts are not strongly influenced by correlation uncertainty.

From the radar chart reported in Fig. 14, it can be observed that Scenario 2 shows an intermediate behavior, whereas Scenarios 1 and 3 exhibit opposite trends for most impact categories. In Scenario 3, emissions increase in all categories where material processing plays a major role. These include freshwater eco-toxicity (FET), freshwater eutrophication (FE), human toxicity carcinogenic and non-carcinogenic (HTC, HTNC), ionizing radiation (IR), and mineral resource depletion. Additional increases are also observed in categories directly linked to the larger photovoltaic installation, such as land use (LU) and water use (WU). On the other hand, Scenario 1 shows higher values in all categories strongly affected by fossil fuel combustion, such as acidification (AT), climate change (GWP), energy resource depletion (ER), marine and terrestrial eutrophication (ME, TE), ionizing radiation (IR), ozone depletion (OD), particulate matter formation (PM), and photochemical oxidant formation (POF). To summarize the overall environmental performance across all impact categories, the results of the single score analysis are presented in Fig. 15, highlighting the contribution of the main categories. The single score confirms the benefits of storing solar energy in the form of compressed air, even though not all categories are improved by the installation of the storage system. The overall impact decreases from $8.38 \cdot 10^{-5}$ Pt/kWh in Scenario 1 to $5.55 \cdot 10^{-5}$ Pt/kWh in Scenario 2, and further down to $2.33 \cdot 10^{-5}$ Pt/kWh in Scenario 3. Fig. 15 also shows that in Scenarios 1 and 2 the dominant contributions come from GWP and resource depletion, both strongly linked to diesel consumption. These categories experience the most pronounced reductions when moving from Scenario 1 to Scenario 3 via Scenario 2. In the final configuration (Scenario 3), the contribution of the different impact categories appears more balanced, with a relative increase in the role of categories associated with material-intensive components, such as mineral resource depletion.

Focusing on Scenario 3, Fig. 16 reports the percentage breakdown of impacts across the midpoint categories. The graph clearly shows

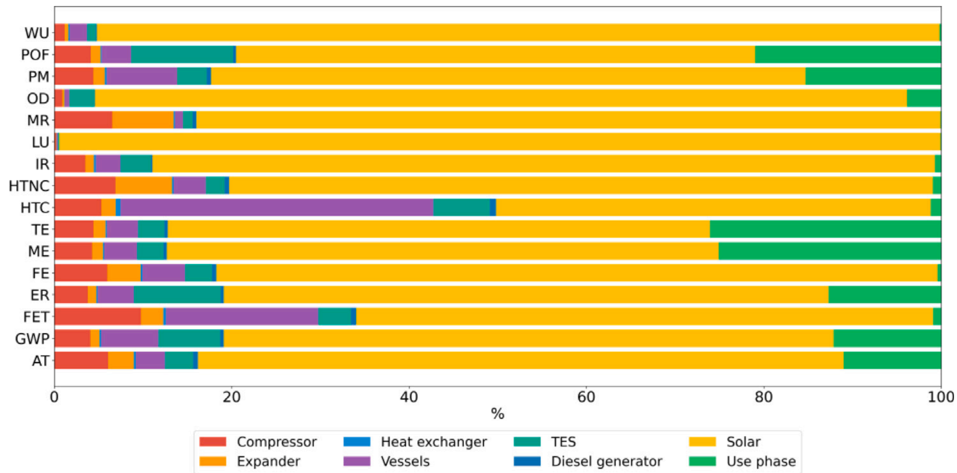

Fig. 16. Percentage breakdown of impacts for midpoint categories.

that a substantial portion of life cycle emissions is attributable to the photovoltaic system. For climate change, approximately 70% of the total impact arises from the production and disposal of silicon panels. This result highlights the strong influence of the storage RTE on the overall environmental performance of the hybrid configuration. Since the minimization of GWP requires limiting the size of the photovoltaic system, improving storage efficiency becomes crucial in order to reduce the amount of electricity that must be generated to compensate for storage losses. Storage systems characterized by limited round-trip efficiency, such as the one considered in this study, lead to increased photovoltaic requirements and therefore negatively affect the environmental performance of the system. Climate altering emissions during the use phase depend on the amount of diesel consumed, with almost all burdens originating from direct combustion. A smaller contribution is linked to diesel production and transport, as well as lubricating oil. The impact of the thermal storage unit derives mainly from mineral oil. About half of its greenhouse gas emissions are associated with the end-of-life stage, as the oil is typically incinerated as hazardous waste, directly releasing greenhouse gases into the atmosphere. The relative contribution of components varies considerably across other impact categories. For terrestrial acidification, the dominant contribution is from the PV installation, particularly from multi-Si cell production. Human toxicity and mineral resource depletion are instead driven by the construction of the CAES system, due to the substantial material requirements. Within human toxicity, the carcinogenic impact is largely attributable to steel production, whereas in the non-carcinogenic case, steel-related emissions are less relevant, and the main contribution shifts to PV cell manufacturing. The fossil energy use category shows the highest burden in the use phase, reflecting diesel consumption, although metalworking remains non-negligible. Particulate matter formation is again dominated by the PV system, with silicon processing as the main hotspot. Finally, land use and water use indicators are almost entirely controlled by PV installation, with land occupation from solar panels representing nearly 100% of the total.

In general terms, Fig. 16 shows that, in Scenario 3, the majority of the environmental impact is attributable to the construction phase of the photovoltaic panels. This result might appear to contradict what is commonly reported in the literature, where LCA studies of CAES systems indicate that the main contribution to the environmental impact arises from the operational phase. However, this apparent discrepancy stems from the definition of the system boundaries adopted in the present LCA study, which include the storage unit, the photovoltaic system, and the diesel generator within the system boundary. Consequently, the results characterize the entire plant responsible for supplying electricity to the end user. If the environmental effects of the CAES unit alone were to be assessed, all emissions associated with the photovoltaic system would be attributed to the operational phase. Under this assumption, the greenhouse gas emissions per kWh of the CAES would amount to 0.212 kg CO_2eq, a higher value than that obtained for Scenario 3, which represents a combined impact associated with the combined operation of the compressed air storage, diesel generator, and photovoltaic generation systems. This value (i.e., 0.212 kgCO_2eq/kWh) is consistent with those reported in the literature for CAES systems operating under electricity mixes with moderate carbon intensity (Oliveira et al., 2015; Kapila et al., 2019). Conversely, the literature addressing the environmental impact of lithium-ion battery energy storage reports generally lower GWP values, typically in the range of 50–150 g CO_2eq/kWh (Gutsch and Leker, 2022; Jasper et al., 2022). These lower values are mainly attributable to the operational phase, as the higher round-trip efficiency of battery systems reduces the amount of electricity required per unit of discharged energy. Nevertheless, CAES systems can mitigate issues related to the extraction and processing of critical raw materials and rare earth elements associated with lithium-ion battery technologies. However, a detailed and systematic comparison between CAES and battery storage technologies is beyond the scope of this work and would require a harmonized life cycle assessment framework, which represents a clear direction for future research.

4.2. Comparison between GWP and single score minimization results

In this section, a comparison is presented between the results obtained when the optimization process is performed using the Single Score (SS) as the objective function instead of minimizing GWP. For brevity, results are reported only for the Zimbabwe case study, already analyzed in more detail in the previous section. This approach provides insights into how the optimal configuration evolves when all midpoint indicators are considered simultaneously. Although GWP remains one of the most widely used indicators in environmental assessments, this comparison helps clarify how system design may change when broader environmental aspects are accounted for. The results, summarized in Table 6, show that the two configurations differ only marginally in terms of both system sizing and environmental impact. Minor deviations are nevertheless observed: in the SS-based solution, the air storage capacity and the PV subsystem are slightly reduced, while machine swept volume remains essentially unchanged. This adjustment results in a lower energy contribution from CAES and a consequent increase in CO_2 emissions from diesel generation. Specifically, GWP increases from 144 to 152 gCO_2eq/kWh, while the Single Score decreases from 2.33×10^{-5} to 2.26×10^{-5}.

The radar chart in Fig. 17 compares the normalized values of all midpoint indicators with respect to their maximum. It clearly shows

Table 6
Minimum GWP and minimum SS configuration.

	$V_{s,c}$ [cm^3]	$V_{s,ex}$ [cm^3]	p_{max} [bar]	V [m^3]	$P_{PV,p}$ [kW$_p$]	GWP $\left[\frac{kg\ CO_2\ eq}{kWh}\right]$	SS [Pt/kWh]
Min GWP	2150	17.0	91	23.1	74	0.144	2.33×10^{-5}
Min SS	2045	16.3	100	18.2	67	0.152	2.26×10^{-5}

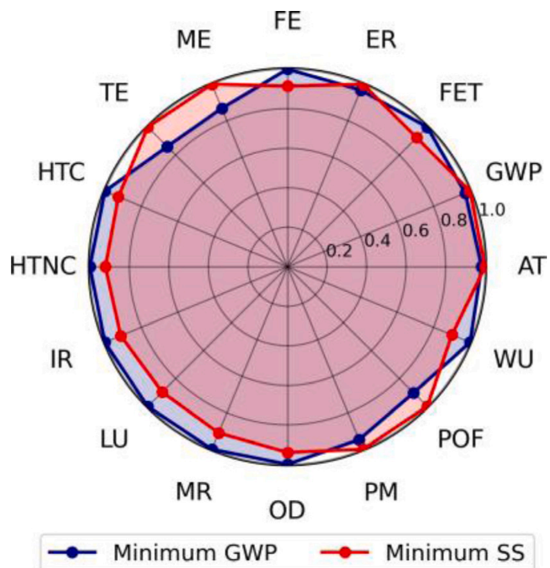

Fig. 17. Midpoint comparison for minimum GWP and minimum SS configuration.

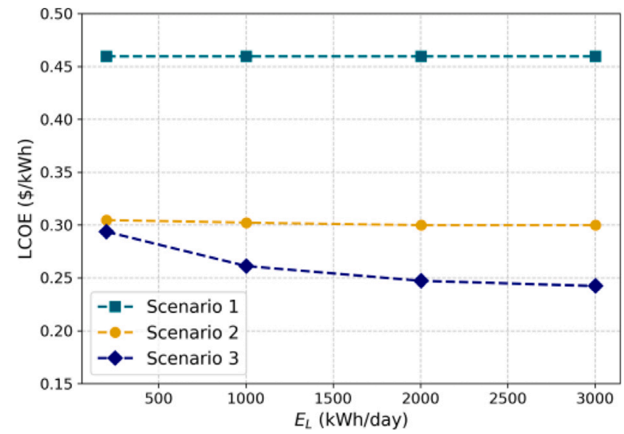

Fig. 18. LCOE for the three scenarios in HPV-HC site at different system scale expressed as user daily energy request.

that differences between the two configurations remain limited, with variations generally within 10% of the maximum value. When the SS is minimized, the reduction in installed PV power and storage volume slightly decreases the impacts of categories mainly associated with metal processing, such as ecotoxicity, eutrophication, and human toxicity; conversely, it leads to an increase in categories that are strongly influenced by direct fuel combustion emissions. Overall, the two optimization approaches, converge towards very similar system configurations. This behavior is largely explained by the relatively high weight attributed to climate change (approximately 20%) in the EF normalization and weighting set. The configuration that minimizes climate change emissions therefore closely corresponds to the one that minimizes the aggregated indicator, reinforcing the robustness of the GWP-based optimization despite the uncertainty of the SS. Importantly, the conclusions drawn in the previous section regarding the comparison of the three scenarios and the contribution of the different CAES components remain valid even if the optimization is performed with the Single Score as the objective function.

4.3. Economic assessment results

An optimization procedure is also carried out to determine the system configuration that minimizes the global LCOE in each scenario. Fig. 18 reports the results obtained for the different scenarios in the most promising location (i.e. Zimbabwe), which is characterized by both high photovoltaic potential and elevated diesel costs, at varying system scales. The different scales, expressed in terms of the total daily user energy demand, were derived by multiplying the base load profile by a specific coefficient. From left to right, the plotted data correspond to peak loads of 11, 55, 110, and 160 kW, respectively. While the LCOE for Scenarios 1 and 2 remains nearly constant with increasing system size, Scenario 3 exhibits a decreasing trend. This behavior is explained by the fact that, whereas the costs of diesel generators and PV modules scale linearly, the cost functions describing CAES equipment are nonlinear, thereby benefiting from economies of scale. Scenario 1 results in the highest LCOE (0.459 $/kWh). At the base system size, the configuration including CAES storage shows a slightly lower LCOE than Scenario 2 (0.294 $/kWh for the former and 0.299 $/kWh for the latter). However, due to the decreasing trend of Scenario 3, for larger system size the integration of CAES becomes clearly cost-effective. The LCOE of Scenario 3 continues to decline, reaching 0.244 $/kWh at 2 MWh/day. At even larger scales, Scenario 3 achieves slightly lower LCOE values and gradually approaches an asymptotic trend. These results indicate that micro-scale compressed air systems have limits of cost-effectiveness for micro-scale off-grid installations. However, they can become more competitive as the system scale increases. In the largest configuration analyzed, the reciprocating compressor included in the system has a rated capacity of approximately 550 kW, which corresponds to the upper limit at which this technology is typically employed. For larger system sizes, the adoption of centrifugal compressors could represent a more suitable solution. A more detailed analysis of the impact of system size should therefore also consider this technological transition, which represents an interesting direction for future investigations.

An analogous analysis was also conducted to evaluate the sensitivity of GWP to system size. Nevertheless, the results are not reported in Section 4.1, as in Scenario 3 the increase in system size leads to a modest reduction in emissions (approximately 3%). This limited variation can be explained by the fact that, although some of the size–mass correlations exhibit sublinear behavior, the largest contribution, as shown in the breakdown in Fig. 16, originates from the photovoltaic system, which is described by linear relationship between mass, and consequently environmental impact, and system size. Moreover, the disparity among the three scenarios is so pronounced that variations associated with system size do not yield any meaningful differences in the overall outcome.

Table 7 summarizes the design and performance parameters of the configurations that minimize GWP and LCOE for Zimbabwe, considering both the smallest and largest system sizes. It is worth noting that, within the range of system sizes analyzed, the significant increase in storage volume suggests that alternative air storage solutions could become technically preferable. As total volumetric capacity grows, relying on a large number of small, standardized pressure vessels may no longer represent the most convenient option from a plant design perspective. In such cases, fewer vessels with larger individual volumes could reduce system complexity and balance-of-plant requirements. However, in the present work no change in storage technology is considered, and the same assumptions adopted at the minimum system size are consistently maintained across all configurations. This choice allows for a coherent

Table 7
Comparison of optimized configurations for Zimbabwe considering either GWP or LCOE as the objective function, for the minimum and maximum analyzed system sizes.

Objective function	E_L $\left[\frac{kWh}{day}\right]$	V [m^3]	$V_{s,c}$ [cm^3]	$V_{s,ex}$ [cm^3]	$P_{PV,p}$ [kW_p]	p_{max} [bar]	RTE [%]	RSS [%]	GWP $\left[\frac{kg\ CO_2\,eq}{kWh}\right]$	LCOE $\left[\frac{\$}{kWh}\right]$
GWP	200	23.1	2150	17	74	91	35.7	98.3	0.144	0.322
	3000	353.2	32 496	250	1146	93	35.4	98.8	0.140	0.287
LCOE	200	13.3	1640	15	69	117	35.1	93.9	0.174	0.294
	3000	203.7	26 106	226	1018	117	35.4	94.4	0.167	0.244

comparison of results, while acknowledging that storage technology selection may influence both cost and system layout as volumetric requirements increase.

A clear distinction emerges between the outcomes associated with the two objective functions, in terms of both design choices and system performance. When cost minimization is targeted, the optimization yields smaller photovoltaic and storage capacities compared with the GWP-minimizing case, at the expense of lower renewable self-sufficiency. The optimization also identifies different storage-pressure values that minimize environmental impact (~90 bar) and system cost (~117 bar). Moreover, while using GWP as the objective function leads to a system size that scales almost linearly with the user's energy demand, the economically optimal configurations exhibit a more-than-linear increase in component size. This behavior is driven by nonlinear cost scaling, whereby several components show sublinear cost growth with increasing capacity. As a result, larger systems achieve slightly higher renewable self-sufficiency (RSS increases from 93.9% to 94.4%) while simultaneously reducing the cost of electricity. This trend is further reflected in Fig. 19, which presents the investment cost breakdown for the LCOE-minimizing configurations. A reduction is observed in the relative contribution of components governed by nonlinear cost functions—particularly the heat exchangers, followed by the compressor and expander. Conversely, the largest cost contributions arise from the photovoltaic system and the pressure vessels, which represent the most expensive component of the CAES system. Fig. 20 shows the economic results obtained for the maximum system size across all seven locations, including an uncertainty bar corresponding to a ±10% variation in diesel price. An economic benefit is observed only for the MPV-HC and LPV-HC location (i.e., Belize and Romania), which are also characterized by high fuel prices. These findings highlight the strong dependence of system performance on diesel cost: the implementation of storage provides slight benefits only in regions with high fuel prices, where minimizing diesel generator usage is advantageous. In countries with lower fuel costs, CAES implementation may not be economically advisable. However, PV installation remains beneficial in all cases when compared to full diesel dependency. The limited competitiveness of compressed air storage systems is mainly attributable to their low round-trip efficiency (approximately 35%–36%), which results in an excessively oversized PV system. Compared with the results presented in Section 4.1, it can be concluded that while solar energy storage offers clear environmental benefits regardless of geographic location, the economic viability of CAES implementation is not necessarily achievable with the present configuration and remains strongly dependent on local economic factors. To contextualize the present results, literature addressing alternative storage technologies can be considered. Similar analyses of hybrid PV–diesel-lithium-ion battery systems report levelized costs of energy in the range of 0.15–0.30$/kWh, indicating generally lower costs, although of the same order of magnitude (Aziz et al., 2022; Khan et al., 2017; Omar, 2025; Salau et al., 2024). As observed for the environmental performance, this difference can be attributed to the lower overall efficiency of CAES-based systems, as well as to the high capital costs of specific components, in particular the compressed air storage tanks.

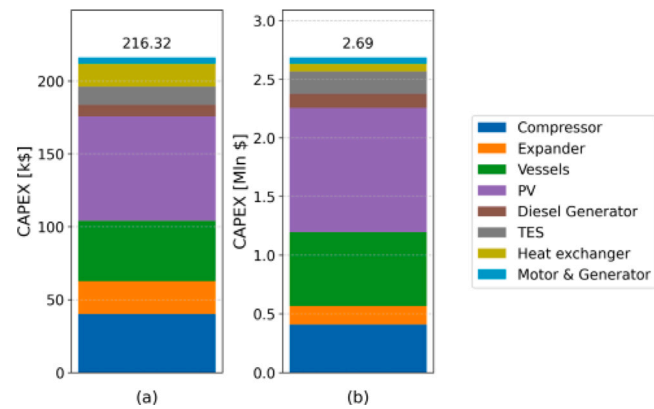

Fig. 19. CAPEX breakdown for configurations that minimize the LCOE for the minimum (a) and maximum (b) analyzed system sizes.

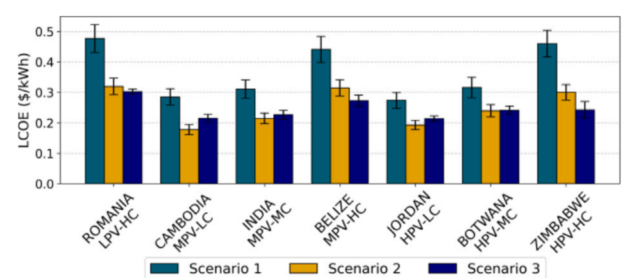

Fig. 20. LCOE for the three scenarios in different geographic site.

5. Conclusion

This study performs a parametric Life Cycle Assessment and techno-economic analysis of hybrid PV–diesel–CAES systems for off-grid power generation across different geographic contexts. The results provide insights into the environmental and economic implications of implementing compressed air energy storage at small scales. Through the parametric approach, the work investigated how design parameters, local solar potential, and fuel costs influence both sustainability and cost-effectiveness.

The main outcomes of the present work can be summarized as follows:

- The study introduces size–power correlations enabling the scaling of reference inventories to better reflect the behavior of commercial components. The uncertainty associated with using these correlations to estimate actual component dimensions was explicitly accounted for and found to be acceptable for the scope of the present analysis. These correlations establish a parametric foundation for future LCA-based assessments.
- CAES integration consistently lowers CO_2 emission. Compared with the diesel-only system (0.996 kg CO_2eq/kWh), the hybrid PV–diesel configuration reduces emissions by approximately one third, while the PV–diesel–CAES system achieves reductions to as low as 0.144 kg CO_2eq/kWh.

- The sequential addition of photovoltaic generation and CAES storage results in an overall improvement in environmental performance, both in terms of Global Warming Potential and aggregated single-score indicators. Nonetheless, higher impacts are observed in categories linked to metal production and raw material extraction (e.g., mineral resource depletion, human toxicity).
- In the PV–diesel–CAES configuration, the photovoltaic subsystem emerges as the dominant contributor to total environmental impact, primarily due to the oversizing required to compensate for the limited round-trip efficiency. This same oversizing also leads to higher capital costs, showing how limited storage efficiency and the resulting increase in photovoltaic capacity simultaneously affect both the environmental and economic performance of the system.
- From an economic perspective, CAES integration is hardly cost-competitive at micro scales (~10 kW), with profitability mainly driven by increased system size and, especially, by installations in regions with high diesel prices, where the fuel substitution benefits outweigh the additional capital expenditure. In most other contexts, the study highlights a clear mismatch between environmental improvement and economic viability under current technological and market conditions. It is worth noting, however, that the current global economic context is characterized by a continuous increase in fossil fuel prices. This trend could make the use of PV–CAES based systems economically attractive in a growing number of installation sites.

Overall, CAES demonstrates strong potential for reducing greenhouse gas emissions in off-grid applications and represents a viable pathway for decarbonizing diesel-dependent communities. However, its economic viability remains constrained at small scales and highly sensitive to local conditions, as the environmental benefits of PV–diesel–CAES systems are closely associated with increased system complexity, photovoltaic oversizing, and capital investment. The pronounced dependence on diesel price, system size, and storage efficiency highlights the need for integrated techno-economic and environmental assessments prior to deployment, since improvements in one dimension do not necessarily translate into benefits in the other.

Despite the comprehensive parametric framework adopted, this study has some limitations. The analysis relies on numerical models with simplifying assumptions, where component performance is described through literature-based correlations assumed valid over the investigated operating range and system lifetime, while long-term effects such as degradation are not explicitly considered. The techno-economic and life cycle assessments are based on representative cost data, market assumptions, and life cycle inventory analogies, making absolute results sensitive to these inputs, although relative trends among scenarios are considered robust.

Future research will extend the parametric analysis to a wider range of system sizes and consider alternative technologies for the compression and expansion stages, particularly at larger scales. In addition, the environmental assessment will be broadened through comparative life cycle analyses with other energy storage technologies, including thermomechanical solutions such as pumped thermal energy storage and electrochemical systems, notably lithium-ion batteries. At the same time, further efforts will be devoted to strengthening the robustness of the proposed LCA framework by refining the life cycle inventory, incorporating uncertainty and data quality analyses, aging-aware modeling approaches capable of accounting for performance degradation and parameter evolution over the system lifetime.

CRediT authorship contribution statement

Dario Tumminello: Writing – original draft, Software, Methodology, Investigation, Formal analysis, Data curation, Conceptualization. **Claudio Zuffi:** Writing – review & editing, Software, Methodology. **Tommaso Bacci:** Writing – review & editing, Writing – original draft, Supervision, Conceptualization. **Bruno Facchini:** Writing – review & editing, Supervision, Funding acquisition.

Declaration of Generative AI use in the writing process

During the preparation of this work, the authors used ChatGPT to improve the readability of the paper. The authors then reviewed and edited the content as needed and take full responsibility for the content of the publication.

Declaration of competing interest

The authors declare that they have no known competing financial interests or personal relationships that could have appeared to influence the work reported in this paper.

Appendix A. Supplementary data

Supplementary material related to this article can be found online at https://doi.org/10.1016/j.cles.2026.100246.

Data availability

Data will be made available on request.

References

Adams, B.M., Bohnhoff, W.J., Dalbey, K.R., Ebeida, M.S., Eddy, J.P., Eldred, M.S., Hooper, R.W., Hough, P.D., Hu, K.T., Jakeman, J.D., et al., 2020. Dakota, a Multilevel Parallel Object-Oriented Framework for Design Optimization, Parameter Estimation, Uncertainty Quantification, and Sensitivity Analysis: Version 6.13 User's Manual. Technical Report, Sandia National Lab.(SNL-NM), Albuquerque, NM (United States).

Adib, M., Nasiri, F., Haghighat, F., 2023. Integrating wind energy and compressed air energy storage for remote communities: A bi-level programming approach. J. Energy Storage 72, 108496.

Alsema, E.A., 2000. Environmental life cycle assessment of solar home systems. Department of Science Technology and Society, Utrecht University Utrecht ....

Alzahrani, K.M., Hee, J.L., Elsakka, M., Ingham, D., Ma, L., Pourkashanian, M., 2024. Techno-economic assessment of vertical axis wind turbine driven ro desalination with compressed air energy storage for remote communities. Desalination 592, 118094.

Arabkoohsar, A., Rahrabi, H.R., Alsagri, A.S., Alrobaian, A.A., 2020. Impact of off-design operation on the effectiveness of a low-temperature compressed air energy storage system. Energy 197, 117176.

Atlas Copco, 2025. Atlas Copco industrial piston compressors. URL https://www.atlascopco.com/en-uk/compressors/products/air-compressor/piston-compressor.

Aziz, A.S., Tajuddin, M.F.N., Zidane, T.E.K., Su, C.-L., Alrubaie, A.J.K., Alwazzan, M.J., 2022. Techno-economic and environmental evaluation of PV/diesel/battery hybrid energy system using improved dispatch strategy. Energy Rep. 8, 6794–6814.

Bauer compressors, (2025). URL https://www.bauer-kompressoren.de/it/.

Bazdar, E., Sameti, M., Nasiri, F., Haghighat, F., 2022. Compressed air energy storage in integrated energy systems: A review.

Blaskmer, 2025. Blackmer LB compressor series. URL https://www.psgdover.com/blackmer/products/reciprocating-gas-compressors/lb-series-reciprocating-gas-compressors.

Bleicher, A., Pehlken, A., 2020. The Material Basis of Energy Transitions. Academic Press.

Boge, 2025. BOGE compressed air systems. URL https://www.boge.com/en/.

Bowman, E., 2025. Heat exchangers and oil coolers. URL https://ej-bowman.com/.

Braimakis, K., Westermeier, M., Schifflechner, C., Beaughon, M., Serafino, A., Charalampidis, A., Karellas, S., 2025. A general framework for part-load optimization of air-cooled ORCs with screw expanders. Energy 137061.

Burckardt, 2025. Burckhardt compression standard high pressure compressors. URL https://www.burckhardtcompression.com/.

Carvalho, J.E.S.P., Pradelle, F., Rullière, R., Revellin, R., 2025. Seasonal assessment of a hybrid CCHP-photovoltaic system coupled with CAES for a residential building in Rio de Janeiro: Energetic, exergetic, exergoeconomic and environmental analysis. Energy Convers. Manage. 329, 119637.

Cassoret, B., Manata, J.-P., Mallard, V., Roger, D., 2019. Comparative life cycle assessment of induction machines made with copper-cage or aluminium-cage rotors. IET Electr. Power Appl. 13 (6), 712–719.

Cheayb, M., Gallego, M.M., Tazerout, M., Poncet, S., 2022. A techno-economic analysis of small-scale trigenerative compressed air energy storage system. Energy 239.

Cioccolanti, L., Hamedani, S.R., Villarini, M., 2019. Environmental and energy assessment of a small-scale solar organic rankine cycle trigeneration system based on compound parabolic collectors. Energy Convers. Manage. 198, 111829.

Cioni, S., Papini, C., Superchi, F., Milazzo, A., Bianchini, A., 2023. Techno-economic analysis of I-CAES systems to increase dispatchability of wind power. In: Journal of Physics: Conference Series, vol. 2648, (1), IOP Publishing, 012004.
Cocco, D., Lecis, L., Micheletto, D., 2023. Life cycle assessment of an integrated PV-ACAES system. Energies 16 (3), 1430.
Congedo, P.M., Baglivo, C., Panico, S., Mazzeo, D., Matera, N., 2022. Optimization of micro-CAES and TES systems for trigeneration. Energies 15.
Couper, J.R., 2005. Chemical Process Equipment: Selection and Design. Gulf professional publishing.
CRI, 2025. C.r.i portable generators. URL https://www.crifluidsystems.com/.
Dawoud, S.M., Lin, X., Okba, M.I., 2018. Hybrid renewable microgrid optimization techniques: A review. Renew. Sustain. Energy Rev. 82, 2039–2052.
Declaye, S., Quoilin, S., Guillaume, L., Lemort, V., 2013. Experimental study on an open-drive scroll expander integrated into an ORC (organic rankine cycle) system with R245fa as working fluid. Energy 55, 173–183.
Dehghani-Sanij, A., Tharumalingam, E., Dusseault, M., Fraser, R., 2019. Study of energy storage systems and environmental challenges of batteries. Renew. Sustain. Energy Rev. 104, 192–208.
Denair, 2025. Denair industrial air compressors. URL https://www.denair.net/.
Deng, Y., Wang, Y., Xing, X., Xiong, Y., Xu, S., Wang, R., 2024. Requirement on the capacity of energy storage to meet the 2°C goal. Sustainability 16 (9), 3753.
Dream Compressor, (2025). URL https://www.dreamcompressor.com/.
Dumont, O., Parthoens, A., Dickes, R., Lemort, V., 2018. Experimental investigation and optimal performance assessment of four volumetric expanders (scroll, screw, piston and roots) tested in a small-scale organic rankine cycle system. Energy 165, 1119–1127.
Dumont, O., Talluri, L., Fiaschi, D., Manfrida, G., Lemort, V., 2019. Comparison of a scroll, a screw, a roots, a piston expander and a tesla turbine for small-scale organic rankine cycle. In: ORC Conference 2019.
Ecoinvent, 2023. Ecoinvent database 3.10. Available online: URL https://ecoinvent.org/ecoinvent-v3-10/.
Elzein, H., Dandres, T., Levasseur, A., Samson, R., 2019. How can an optimized life cycle assessment method help evaluate the use phase of energy storage systems? J. Clean. Prod. 209, 1624–1636.
Endüstriyel, E., 2025. Ekin industrial accumulator tanks. https://en.ekinendustriyel.com.
Fajinmi, O., Munda, J.L., Hamam, Y., Popoola, O., 2023. Compressed air energy storage as a battery energy storage system for various application domains: a review. Energies 16 (18), 6653.
Fini compressors, 2024. OS series compressors catalogue. URL https://finicompressors.com/wp-content/uploads/Catalogo-OS_Fini_IT_04-2024_9990392.pdf.
Fritzson, P., Aronsson, P., Lundvall, H., Nyström, K., Pop, A., Saldamli, L., Broman, D., 2005. The openmodelica modeling, simulation, and software development environment. Simul. News Eur. 44, 8–16.
Giuffrida, A., 2017. Improving the semi-empirical modelling of a single-screw expander for small organic rankine cycles. Appl. Energy 193, 356–368.
GlobalPetrolPrices, 2025. Diesel prices. URL https://it.globalpetrolprices.com/diesel_prices/. (Accessed 27 August 2025).
Gnana, K., 2017. Lazard's Levelized Cost of Energy Analysis—Version 11.0. Report, Lazard, URL https://www.lazard.com/perspective/levelized-cost-of-energy-2017/.
Green power generators, (2025). URL https://www.greenpowergen.it/.
Greening, B., Azapagic, A., 2014. Domestic solar thermal water heating: A sustainable option for the UK? Renew. Energy 63, 23–36.
Gutsch, M., Leker, J., 2022. Global warming potential of lithium-ion battery energy storage systems: A review. J. Energy Storage 52, 105030.
He, Y., Guo, S., Dong, P., Zhang, Y., Huang, J., Zhou, J., 2023. A state-of-the-art review and bibliometric analysis on the sizing optimization of off-grid hybrid renewable energy systems. Renew. Sustain. Energy Rev. 183, 113476.
He, W., Wang, J., 2018. Optimal selection of air expansion machine in compressed air energy storage: A review.
Heidari, M., Parra, D., Patel, M.K., 2021. Physical design, techno-economic analysis and optimization of distributed compressed air energy storage for renewable energy integration. J. Energy Storage 35, 102268.
Ibrahim, H., Ilinca, A., 2012. Contribution of the compressed air energy storage in the reduction of ghg-case study: Application on the remote area power supply system. In: Air Pollution-a Comprehensive Perspective. IntechOpen.
Ibrahim, H., Younès, R., Ilinca, A., Dimitrova, M., Perron, J., 2010. Study and design of a hybrid wind–diesel-compressed air energy storage system for remote areas. Appl. Energy 87 (5), 1749–1762.
Ielang, 2025. Ielang, PM VSD screw compressor. URL https://www.ielang.net/pm-vsd-screw-compressor-15585048500673852.html.
I.E.S. Group, 2025. IES Thermal energy storage. https://ies-group.com.hk.
International Organization for Standardization, 2006. Environmental Management: Life Cycle Assessment; Principles and Framework. ISO.
Jasper, F.B., Späthe, J., Baumann, M., Peters, J.F., Ruhland, J., Weil, M., 2022. Life cycle assessment (LCA) of a battery home storage system based on primary data. J. Clean. Prod. 366, 132899.
Jones, D.R., Schonlau, M., Welch, W.J., 1998. Efficient global optimization of expensive black-box functions.
Joshi, K., 2017. Sustainable energy systems with photovoltaic generation and energy storage solutions for rural communities in India and Canada.
Kabir, M.R., Rooke, B., Dassanayake, G.M., Fleck, B.A., 2012. Comparative life cycle energy, emission, and economic analysis of 100 kW nameplate wind power generation. Renew. Energy 37 (1), 133–141. http://dx.doi.org/10.1016/j.renene.2011.06.003.
Kaishan USA, 2025. Rotary screw air compressors. URL https://kaishanusa.com/rotary-screw-air-compressors/.
Kapila, S., Oni, A., Gemechu, E., Kumar, A., 2019. Development of net energy ratios and life cycle greenhouse gas emissions of large-scale mechanical energy storage systems. Energy 170, 592–603.
Kawajiri, K., Oozeki, T., Genchi, Y., 2011. Effect of temperature on PV potential in the world. Environ. Sci. Technol. 45 (20), 9030–9035.
Khan, M.J., Yadav, A.K., Mathew, L., 2017. Techno economic feasibility analysis of different combinations of PV-wind-diesel-battery hybrid system for telecommunication applications in different cities of punjab, India. Renew. Sustain. Energy Rev. 76, 577–607.
King, M., Jain, A., Bhakar, R., Mathur, J., Wang, J., 2021. Overview of current compressed air energy storage projects and analysis of the potential underground storage capacity in India and the UK. Renew. Sustain. Energy Rev. 139.
Kodsan, 2025. Kodsan water heaters and storage tanks. https://kodsan.com.tr.
Lashgari, F., Babaei, S.M., Pedram, M.Z., Arabkoohsar, A., 2022. Comprehensive analysis of a novel integration of a biomass-driven combined heat and power plant with a compressed air energy storage (CAES). Energy Convers. Manage. 255, 115333.
Lazard, 2023. Lazard's Levelized cost of energy analysis—version 16.0. URL https://www.lazard.com/media/typdgxmm/lazards-lcoeplus-april-2023.pdf.
Li, D., Duan, L., 2023. Techno-economic analysis of solar aided liquid air energy storage system with a new air compression heat utilization method. Energy Convers. Manage. 278, 116729.
Li, P., Hu, Q., Li, G., Wang, B., Bai, Y., Han, X., Han, Z., 2022. Research on thermo-economic characteristics of a combined cooling, heating and power system based on advanced adiabatic compressed air energy storage. J. Energy Storage 47, 103590.
Li, Y., Sciacovelli, A., Peng, X., Radcliffe, J., Ding, Y., 2016. Integrating compressed air energy storage with a diesel engine for electricity generation in isolated areas. Appl. Energy 171, 26–36.
Liu, J., Zhang, X., Xu, Y., Chen, Z., Chen, H., Tan, C., 2014. Economic analysis of using above ground gas storage devices for compressed air energy storage system. J. Therm. Sci. 23 (6), 535–543.
Lyons, W.C., Plisga, G.J., 2011. Standard Handbook of Petroleum and Natural Gas Engineering. Elsevier.
McKenna Boiler, 2025. Feedwater Systems. https://www.mckennaboiler.com/feedwater-systems/. (Accessed 26 August 2025).
Mohamad, C., Mylène, M.G., Sébastien, P., Mohand, T., 2019. Micro-scale trigenerative compressed air energy storage system: Modeling and parametric optimization study. J. Energy Storage 26, 100944.
Mohler, D., Sowder, D., 2017. Energy storage and the need for flexibility on the grid. In: Renewable Energy Integration. Elsevier, pp. 309–316.
Oliveira, L., Messagie, M., Mertens, J., Laget, H., Coosemans, T., Van Mierlo, J., 2015. Environmental performance of electricity storage systems for grid applications, a life cycle approach. Energy Convers. Manage. 101, 326–335.
Omar, M.A., 2025. Techno-economic analysis of PV/diesel/battery hybrid system for rural community electrification: A case study in the northern west bank. Energy 317, 134770.
Omec, 2025. Omec motors, electric motor catalogue. URL https://www.omecmotors.com.
Openlca, (2025). URL https://www.openlca.org.
Orange1, 2025. Orange1 asynchronous vectorial motors. URL https://www.orange1.eu/en/all-products/asynchronous-vectorial-motor-mq-series.
Ouyang, T., Zhao, Z., Zhang, M., Xie, S., Wang, Z., 2022. A micro off-grid power solution for solid oxide fuel cell waste heat reusing enabled peak load shifting by integrating compressed-air energy storage. Appl. Energy 323, 119589.
Petrov, M.P., Arghandeh, R., Broadwater, R., 2013. Concept and application of distributed compressed air energy storage systems integrated in utility networks. In: ASME Power Conference, http://dx.doi.org/10.1115/POWER2013-98113, V002T09A004.
Pilan, J., 2025. Pressure vessels and industrial equipment. URL https://www.jpilan.com/.
Pramac, 2025. Pramac energy generation. URL https://www.pramac.com/.
Rahbari, H.R., Arabkoohsar, A., Nielsen, M.P., Mathiesen, B.V., Lund, H., 2021. Quantification of realistic performance expectations from trigeneration CAES-ORC energy storage system in real operating conditions. Energy Convers. Manage. 249, 114828.
Rahman, M.M., Oni, A.O., Gemechu, E., Kumar, A., 2020. Assessment of energy storage technologies: A review. Energy Convers. Manage. 223, 113295.
Raynolds, M., Checkel, M., Fraser, R., 1999. Application of Monte Carlo analysis to life cycle assessment. SAE Trans. 1–9.
Saini, V., Singal, S., 2024. Design and optimization of an off-grid integrated renewable energy system for remote rural electrification in India. Microsyst. Technol. 30 (9), 1201–1215.

Salau, A.O., Maitra, S.K., Kumar, A., Mane, A., Dumicho, R.W., 2024. Design, modeling, and simulation of a PV/diesel/battery hybrid energy system for an off-grid hospital in Ethiopia. E-Prime-Advances Electr. Eng. Electron. Energy 8, 100607.
Sarmast, S., Sejourne, S., Wigston, A., Fraser, R.A., Dusseault, M.B., 2024. Adaptive hybrid energy system for remote Canadian communities: Optimizing wind-diesel systems integrated with adiabatic compressed air energy storage. Energy Convers. Manage. 315, 118778.
Sauer compressors, (2025). URL https://www.sauercompressors.com/.
Smith, A., 2025. A. O. Smith commercial storage tanks. https://www.hotwater.com.
Söltzer, L., Wortmann, B., Stolten, D., Linßen, J., Heinrichs, H., 2026. Material bottlenecks of batteries within the energy transition. Resour. Conserv. Recycl. 227, 108745.
Standard, I., 2006. Environmental management-life cycle assessment-requirements and guidelines. London: ISO.
Sunceter, 2025. Suncenter high pressure compressors. URL https://www.suncentergroup.com/.
Tumminello, D., Bacci, T., Facchini, B., 2024. Numerical modeling and design optimization of a micro-caes system.
Unical, 2025. Unical SRC. https://www.unicalag.it.
Valsteam ADCA, 2025. ADCA Therm. https://www.valsteam.com/.
Weil, M., Ziemann, S., 2014. Recycling of traction batteries as a challenge and chance for future lithium availability. In: Lithium-Ion Batteries. Elsevier, pp. 509–528.
Weis, T.M., Ilinca, A., 2008. The utility of energy storage to improve the economics of wind–diesel power plants in Canada. Renew. Energy 33 (7), 1544–1557.
Wu, S., Zhou, C., Doroodchi, E., Moghtaderi, B., 2020. Techno-economic analysis of an integrated liquid air and thermochemical energy storage system. Energy Convers. Manage. 205, 112341.
Xu, B.B., Jiang, Y., Liu, T.X., Guo, Z., Yu, G., Titirici, M.-M., 2022. Beyond lithium: a new era of sustainable energy engineering.
Xue, H., White, A., 2018. A comparative study of liquid, solid and hybrid adiabatic compressed air energy storage systems. J. Energy Storage 18, 349–359.
Yanmar, 2025. Yanmar diesel generators. URL https://www.yanmar.com/.
Zakeri, B., Syri, S., 2015. Electrical energy storage systems: A comparative life cycle cost analysis. Renew. Sustain. Energy Rev 42 (2015), 569–596.
Zhang, X., Qin, C.C., Xu, Y., Li, W., Zhou, X., Li, R., Huang, Y., Chen, H., 2021. Integration of small-scale compressed air energy storage with wind generation for flexible household power supply. J. Energy Storage 37, 102430.
Zhang, X., Xu, Y., Xu, J., Sheng, Y., Zuo, Z., Liu, J., Chen, H., Wang, Y., Huang, Y., 2017. Study on the performance and optimization of a scroll expander driven by compressed air. Appl. Energy 186, 347–358.
Zhao, Y., Liu, G., Li, L., Yang, Q., Tang, B., Liu, Y., 2019. Expansion devices for organic rankine cycle (ORC) using in low temperature heat recovery: A review. Energy Convers. Manage. 199, 111944.
Zhao, P., Xu, W., Zhang, S., Wang, J., Dai, Y., 2020. Technical feasibility assessment of a standalone photovoltaic/wind/adiabatic compressed air energy storage based hybrid energy supply system for rural mobile base station. Energy Convers. Manage. 206, 112486.
Zheng, Y., Guo, H., Zhang, H., Guo, W., Zhao, M., Xu, Y., Huang, J., Chen, H., 2025. A review of micro compressed air energy storage: Applications, component selection, and dynamic modeling. J. Energy Storage 137, 118614.